Probing Molecular Wires: Synthesis, Structural, and Electronic Study of Donor–Acceptor Assemblies Exhibiting Long-Range Electron Transfer

Francesco Giacalone,[a] José L. Segura,[a] Nazario Martín,*[a] Jeff Ramey,[b] and Dirk M. Guldi*[b]

Abstract: A series of donor–acceptor arrays (C_{60}–oligo-PPV–exTTF; **16**–**20**) incorporating π-conjugated oligo(phenylenevinylene) wires (oligo-PPV) of different length between π-extended tetrathiafulvalene (exTTF) as electron donor and C_{60} as electron acceptor has been prepared by multistep convergent synthetic approaches. The electronic interactions between the three electroactive species present in **16**–**20** were investigated by UV-visible spectroscopy and cyclic voltammetry (CV). Our studies clearly show that, although the C_{60} units are connected to the exTTF donors through a π-conjugated oligo-PPV framework, no significant electronic interactions are observed in the ground state. Interestingly, photoinduced electron-transfer processes over distances of up to 50 Å afford highly stabilized radical ion pairs. The measured lifetimes for the photogenerated charge-separated states are in the range of hundreds of nanoseconds (~500 ns) in benzonitrile, regardless of the oligomer length (i.e., from the monomer to the pentamer). A different lifetime (4.35 μs) is observed for the heptamer-containing array. This difference in lifetime has been accounted for by the loss of planarity of the oPPV moiety that increases with the wire length, as established by semi-empirical (PM3) theoretical calculations carried out with **19** and **20**. The charge recombination dynamics reveal a very low attenuation factor ($\beta = 0.01 \pm 0.005$ Å^{-1}). This β value, as well as the strong electron coupling ($V \sim 5.5$ cm^{-1}) between the donor and the acceptor units, clearly reveals a nanowire behavior for the π-conjugated oligomer, which paves the way for applications in nanotechnology.

Keywords: donor–acceptor systems · electron transfer · fullerenes · nanostructures · oligo(phenylenevinylene)

Introduction

The composition, the interchromophore separation/angular relationship, the overall dynamical and stimulus-induced reorganization, and the electronic coupling are crucial factors in the development of charge-transfer reaction centers.[1] Of particular interest are artificial model systems in which the introduction of simple molecular changes is used to control and tune the magnitude of the electron-transfer parameters. In this context, molecular chains or bridges provide endless opportunities, since they determine not only the structural features but also the size of the electronic coupling matrix element, V, between the donor and acceptor fragments.[2] An important characteristic of a spacer is the possibility of introducing a systematic alteration of separation, orientation, and overlap without affecting the electronic nature of the donor–acceptor pair, for which the coupling is proportional to the overlap of their electronic clouds.[3] Important incentives for this work stem from nature, in which for photosynthetic reaction centers,[4] redox proteins,[5] membranes,[6] and nucleic acids,[7] this relationship has been recognized to control key biological steps/processes. In addition, emerging technologies, such as molecular electronics/preparation of molecular devices, are, in part, based on similar paradigms.[8]

The electron-transfer processes in single molecules have been investigated in some detail, and different mechanisms have been considered which mainly depend on molecular size and structure, as well as the temperature and the free-

[a] Dr. F. Giacalone, Dr. J. L. Segura, Prof. Dr. N. Martín
Departamento de Química Orgánica
Facultad de Ciencias Químicas, Universidad Complutense
28040 Madrid (Spain)
Fax: (+34) 91-394-4103
E-mail: nazmar@quim.ucm.es

[b] J. Ramey, Prof. Dr. D. M. Guldi
Institute for Physical and Theoretical Chemistry
University of Erlangen, 91058 Erlangen (Germany)
Fax: (+49) 913-185-28307
E-mail: dirk.guldi@chemie.uni-erlangen.de

Supporting information for this article is available on the WWW under http://www.chemeurj.org/ or from the author.

 DOI: 10.1002/chem.200500073

energy difference between the donor and acceptor in donor–bridge–acceptor systems. Several different mechanisms, ranging from coherent tunneling or superexchange to thermally activated electron transfer by hopping mechanisms, are particularly relevant to molecular wires, and complete discussions are available in several reviews to which the reader is referred.[9]

Currently, monodisperse and soluble π-conjugated oligomers with a well-defined length and composition are receiving growing interest for the design/integration of molecular wires[10] and rods,[11] since they can be used as tunable building blocks[12] for nanoscale chemical entities in molecular and supramolecular electronic and photonic devices.[13] In this context, electronic conduction along "nanowires" is a key feature of nanochemistry and nanotechnology.[14]

Among the different π-conjugated oligomers, oligo(*p*-phenylenevinylene)s (oligo-PPVs) have been probed as versatile model systems for poly(*p*-phenylenevinylene) derivatives and as novel materials with chemically tailored properties.[15] Much to our surprise, intramolecular electron transfer along conjugated chains of PPV oligomers has been investigated in only a few cases—pentameric oligo-PPV with terminal pentamethylated ferrocene units,[16] or hexameric oligo-PPV bearing two porphyrin groups in the terminal positions.[17]

More recently, a systematic study in which a tetracene donor unit and pyromellitimide acceptor are connected through an oligo-PPV of increasing length (TET–oPPV–PYR) (TET = tetracene, PYR = pyromellitimide) has been reported,[18] thus demonstrating the importance of energy matching between the donor and bridge components for achieving molecular-wire behavior. Quantum-chemical calculations showed a competition between a direct superexchange process and a two-step "bridge-mediated" process whose efficiency depends primarily on the length and nature of the conjugated bridge.[19]

We have recently reported different C_{60}–exTTF[20] (exTTF = π-extended tetrathiafulvalene) and C_{60}–exTTF–exTTF donor–acceptor arrays,[21] which, upon visible light irradiation, undergo cascades of short-range electron-transfer reactions transforming the adjacent radical ion pairs in C_{60}–exTTF–exTTF to distant radical ion pairs. A common characteristic of these donor (i.e., exTTF) acceptor (i.e, C_{60}) arrays is that remarkable effects concerning the lifetime of the charge-separated radical ion pair states evolve. For example, values are observed that reach into the time domain of milliseconds, which has never previously been accomplished in molecular triads. The unique delocalization of electrons provided by the three-dimensional structure of the fullerene core, in combination with the small reorganization energy of C_{60} in electron-transfer reactions, prevents a fast charge-recombination process in these donor–acceptor arrays. This benefit is further augmented by probing a donor system (i.e., exTTF), which, upon charge separation, leads to a gain of aromaticity and planarity of the oxidized fragment. In complementary work we focused on the electron-transfer chemistry of different C_{60}-π-conjugated oligomers[22] and dendrimers.[23]

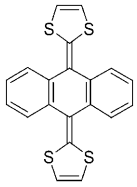

exTTF

We describe here a new series of structurally well-defined donor–acceptor arrays that incorporate a π-extended tetrathiafulvalene (exTTF) as electron donor and fullerene (C_{60}) as electron acceptor, linked by a number of *p*-phenylenevinylene oligomers (oligo-PPV) to yield C_{60}–oligo-PPV–exTTF. Previous work has documented the myriad benefits of testing exTTF/C_{60} donor–acceptor couples. In the current work we take this example one step further and concentrate on the following new aspects. Firstly, a systematic variation

Abstract in Spanish: *Mediante una aproximación sintética convergente en varios pasos, se ha preparado una serie de sistemas dador–aceptor (C_{60}–oligo-PPV–exTTF) (**16**–**20**) incorporando cables moleculares π-conjugados de oligo(fenilenvinileno) (oligo-PPV) de diferente longitud entre la unidad de tetratiafulvaleno π-extendido (exTTF) como dador de electrones y C_{60} como unidad aceptora. Las interacciones electrónicas entre las tres especies electroactivas presentes en **16**–**20** fueron investigadas por espectroscopia UV-Vis y experimentos de voltamperometría cíclica (CV). Nuestros estudios muestran que, aunque las unidades de C_{60} están conectadas a los dadores exTTF a través de un esqueleto π-conjugado de oligo-PPV, no se observan interacciones electrónicas significativas en el estado fundamental. Interesantemente, los procesos de transferencia electrónica fotoinducida a distancias de hasta 50 Å forman pares ion radical altamente estabilizados. Los tiempos de vida medidos para los estados fotogenerados de separación de carga están en el rango de cientos de nanosegundos (~500 ns) en benzonitrilo, independientemente de la longitud del oligómero (desde el monómero al pentámero). Un tiempo de vida diferente (4.35 μs) se ha observado para el sistema que contiene el heptámero. Esta diferencia en el tiempo de vida se ha justificado mediante la pérdida de planaridad del fragmento de oPPV, la cual aumenta con el aumento de la longitud del oligómero, según los cálculos teóricos semiempíricos (PM3) llevados a cabo para **19** y **20**. La dinámica de recombinación de carga revela un factor de atenuación muy bajo ($\beta = 0.01 \pm 0.005$ Å^{-1}). Este valor de β así como el fuerte acoplamiento electrónico ($V \sim 5.5$ cm^{-1}) entre las unidades dadora y aceptora muestran claramente un comportamiento de nanocable molecular para el oligómero π-conjugado, abriendo así el camino a su aplicación en nanotecnología.*

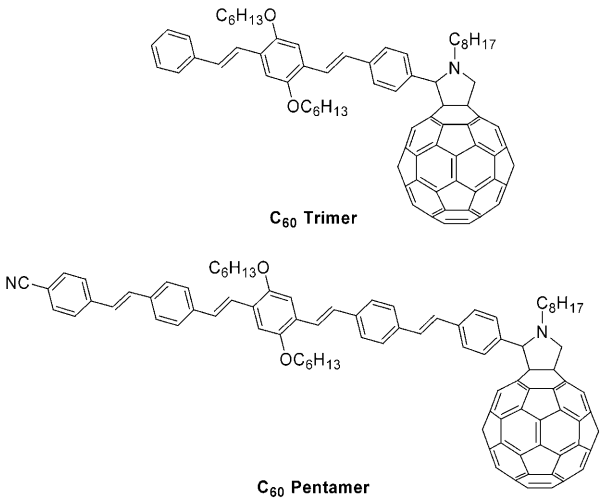

of the oligo-PPV conjugation length.[24] Secondly, conjugating the exTTF moiety with the oligomeric bridge, thus favoring the electronic coupling between them. Thirdly, determining and evaluating the structural and electronic effects of distance and the rates with which the electron/hole transfer through oligo-PPV fragments. Finally, testing the molecular-wire behavior in oligo-PPV-based donor–acceptor systems.

Results and Discussion

Oligo-*p*-phenylenevinylenes (oligo-PPV) of higher molecular weight are intractable.[25] To overcome this general drawback, we prepared a homologous series of oligo-PPVs (**3**, **6**, and **8**) with defined structure and chain length that carry alkoxy chains at the phenylene units to enhance solubility and formyl groups at the termini to allow further chemical transformations.

The target oligo-PPVs were obtained from 2,5-bis(dimethylphosphonatomethyl)-1,4-dihexyloxybenzene (**1**) by Wittig–Horner olefination of suitable functionalized aldehydes. Scheme 1 sketches the general approach to the target oligo-PPVs. For example, formyl-functionalized **3** was obtained by reacting bis-phosphonate **1** with two equivalents of **2**, followed by hydrolysis under acidic conditions. The *p*-phenylenevinylene pentamer **5**, bearing cyano groups at the terminal positions, was prepared from **3** by twofold reaction with phosphonate **4**[26] in 96% yield. Final treatment with DIBAL-H afforded the diformyl-substituted pentamer **6**, which was isolated after flash chromatography in 54% yield. On the other hand, treatment of the diethylketal of terephthaldehyde (**2**) with an excess of bis-phosphonate **1** led, under basic conditions, to **7**, in 41% yield, as a yellow oil. Suitably functionalized heptamer **8** was prepared from previously synthesized building blocks (i.e., **3** and **4**): Wittig–Horner olefination of stoichiometric amounts (2:1) and acid hydrolysis resulted in a stable, orange solid in 77% yield. The presence of up to six solubilizing alkoxy chains provides

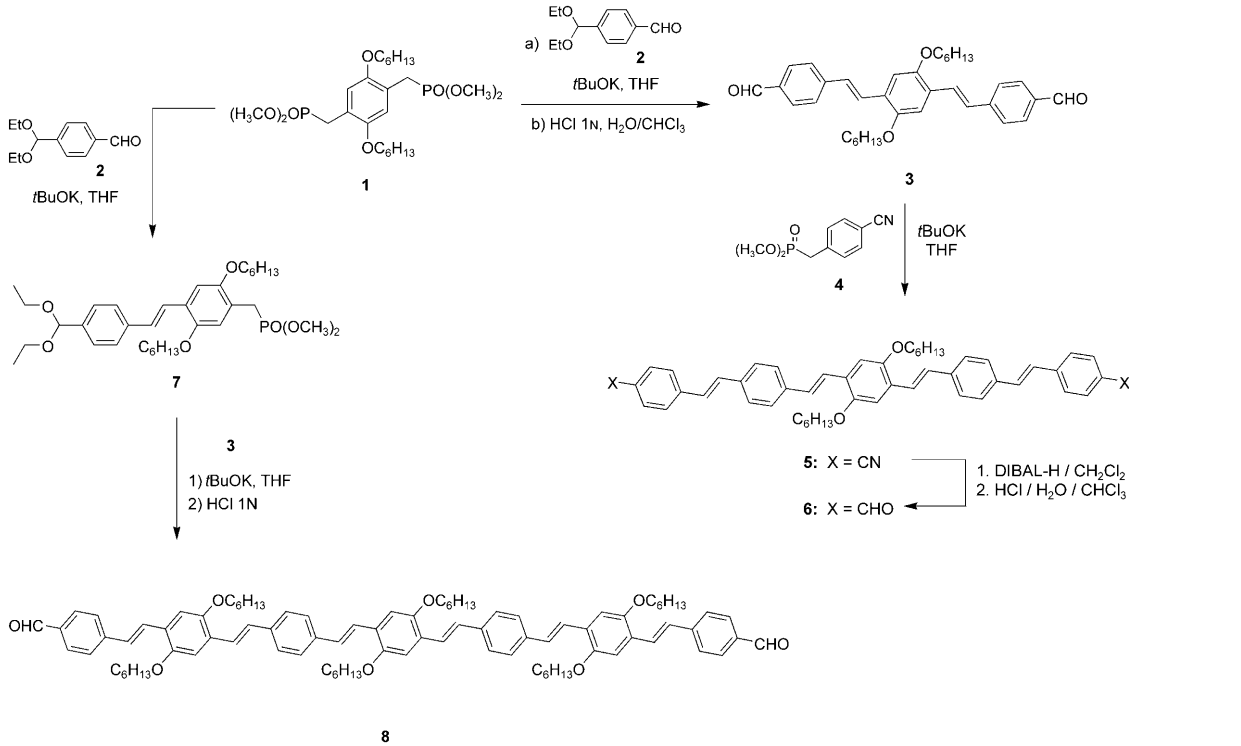

Scheme 1.

good solubility of all target oligo-PPVs, which allows their full spectroscopic characterization (Scheme 1).

Compound **7** emerged as an important building block for controlling the length of the oligo-PPV system in two or four units as well as the integration of versatile formyl groups at the terminal positions. Another benefit of our approach is that the purification of **7** allows the recovery of unreacted starting material (**1**) and the diethylketal of trimer **3**.

A number of spectroscopic techniques were used to determine the structures of the synthesized oligo-PPVs. The FTIR spectra show the cyano and carbonyl groups at around 2225 and 1690–1700 cm^{-1}, respectively, as well as the *trans* substituted double bonds in the region of 960 cm^{-1}. The *E* configuration was confirmed by ^1H NMR spectroscopy: the olefinic protons give rise to two doublets at $\delta \sim 7.6$ and 7.2 ppm with ^3J coupling constants of about 16.5 Hz. In addition, the ^1H NMR spectra also contain signals for the protons of the formyl groups (singlets at about $\delta = 10$ ppm). In the ^{13}C NMR spectra, the signals of the formyl groups are observed at $\delta \sim 191$ ppm. Additional analytical and mass spectroscopic data confirmed the proposed structures.[27]

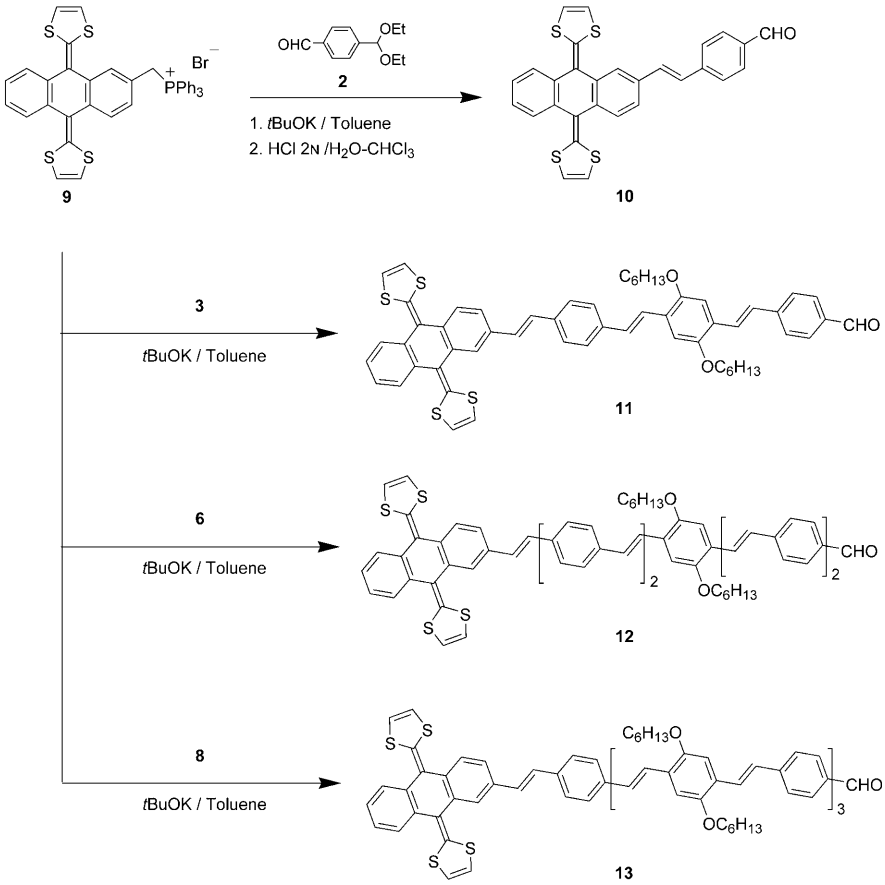

Scheme 2.

In the next phase of our synthetic work-up, Wittig olefination was carried out to link π-extended tetrathiafulvalenes (exTTF) to the respective oligo-PPVs (**2**, **3**, **6**, and **8**). A careful stoichiometric control of triphenylphosphonium bromide **9** and the respective formyl derivatives is particularly important (see Scheme 2).

Phosphonium salts, especially those that are based on exTTF, are very valuable building blocks for this task. They were prepared by refluxing 9,10-bis(1,3-dithiol-2-ylidene)-2-hydroxymethyl-9,10-dihydroanthracene[28] and triphenylphosphane hydrobromide.[21] Then, with toluene as solvent and potassium *tert*-butoxide as base, Wittig reaction of phosphonium salt **9** and the aldehydes **2**, **3**, **6**, and **8** gave **10**–**13**, respectively. An alternative route was pursued for compound **10**; that is, treating **9** with ketal **2** followed by acid hydrolysis to generate the aldehyde groups.

Since Wittig reactions of triphenylphosphonium benzylides with aldehydes afford mixtures of (*Z*)- and (*E*)-alkenes nonstereospecifically,[29] **10**–**13** were obtained as crude products containing the all-*trans* isomers contaminated with small amounts of the corresponding *cis-trans* analogues. Pure *all-trans* **10**–**13** were separated by chromatographic means.[30]

Compound **15**, on the other hand, was prepared by the Wittig–Horner reaction of formyl-exTTF (**14**)[31] and phosphonate **7**. Subsequent acid hydrolysis gave **15** as the all-*trans* conformer (Scheme 3).

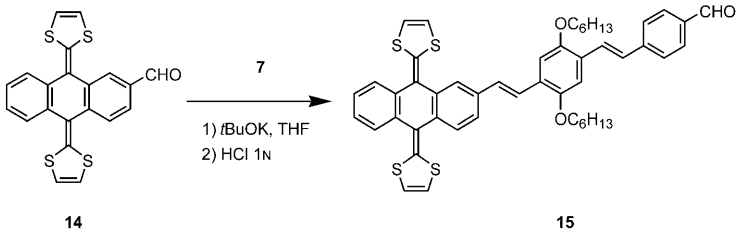

Scheme 3.

Compounds **10**–**13** and **15** were fully characterized on the basis of analytical and spectroscopic data. Importantly, they show, in addition to the oligo-PPV features (vide supra), the presence of exTTF. For example, the ^1H NMR spectra contain singlets at around $\delta = 6.3$ ppm that correspond to the protons of the 1,3-dithiole rings.

Treatment of monoaldehydes **10**–**13** and **15** with C_{60} and sarcosine (*N*-methylglycine), *N*-(3,6,9-trioxadecyl)glycine, or *N*-octylglycine in refluxing toluene or chlorobenzene for 24 h afforded the respective final products in moderate yields. This reaction, as outlined in Scheme 4, takes place by 1,3-dipolar cycloaddition of azomethyne ylides, generated in situ, to C_{60}, according to Prato's protocol,[32] to give **16**–**20** as highly soluble brown solids in 17–47 % yields.

The coupling constants of ~16.5 Hz derived from the ^{1}H NMR spectra of **16**–**20** in $CDCl_3$ attest that the cycloaddition reactions have no appreciable impact on the stereochemistry of the vinyl double bonds. In **18** and **19**, however, overlapping multiplets prevent the accurate determination of the coupling constants. All the ^{13}C NMR spectra show the characteristic signals that correspond to the sp^3 carbon atoms of the pyrrolidine ring (between $\delta = 70$ and 80 ppm) and the tetragonal carbons of the solubilizing alkoxy chains.

For electrochemical and photophysical studies, reference compounds **23**, **25**, and **26** were synthesized, as outlined in Scheme 5. Trimer **23**[33] was prepared similarly to **3**, namely by a Wittig–Horner reaction between bis-phosphonate **1** and benzaldehyde (**21**), whereas pentamer **25** and heptamer **26** were prepared from **3** by olefination reactions with phosphonium salt **24** and phosphonate **22**, respectively. The stilbenic phosphonate **22** was prepared by following a synthetic strategy analogous to that employed for the synthesis of **7**—treatment of **1** with benzaldehyde (**21**) in a 2:1 stoichiometry. Although pentamer **25** was obtained as an isomeric *Z*/*E* mixture, thermal treatment in the presence of iodine yielded the all-*E* stereoisomer quantitatively.

The electronic absorption spectra of the novel systems reveal the characteristics of all components—C_{60}, exTTF, and oligo-PPV. Figure 1 (top) compares, as a representative example, the UV-visible spectrum of **19** with those of the different building blocks, namely exTTF, **25**, and unsubstituted *N*-methylfulleropyrrolidine (**27**).

Bathochromic shifts ranging from 8 to 23 nm were observed when comparing **16**–**20** with the respective oligo-PPV

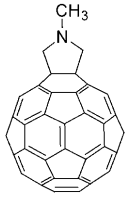

27

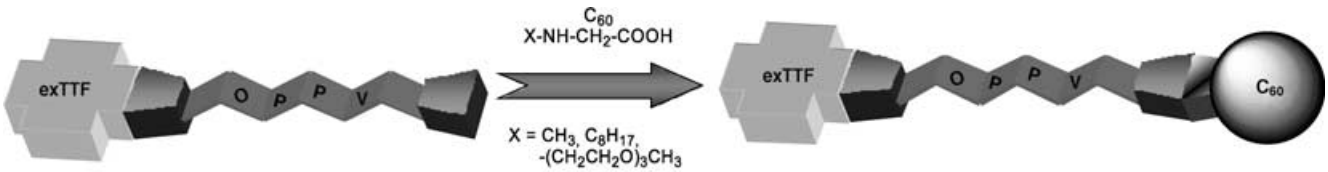

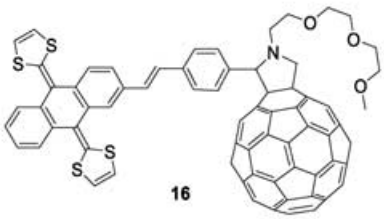

16

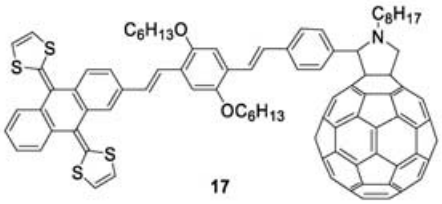

17

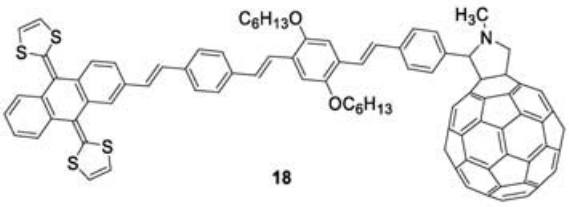

18

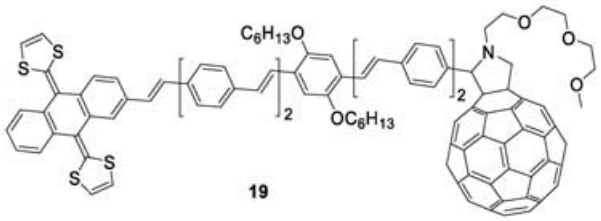

19

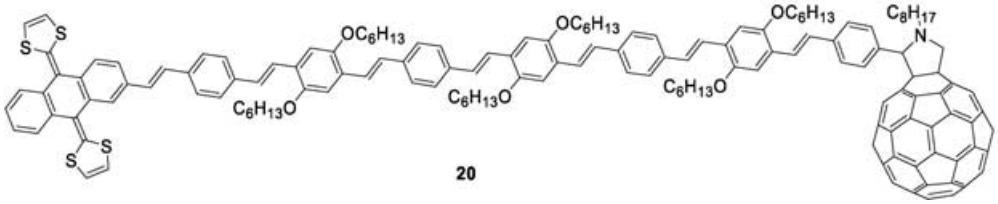

20

Scheme 4.

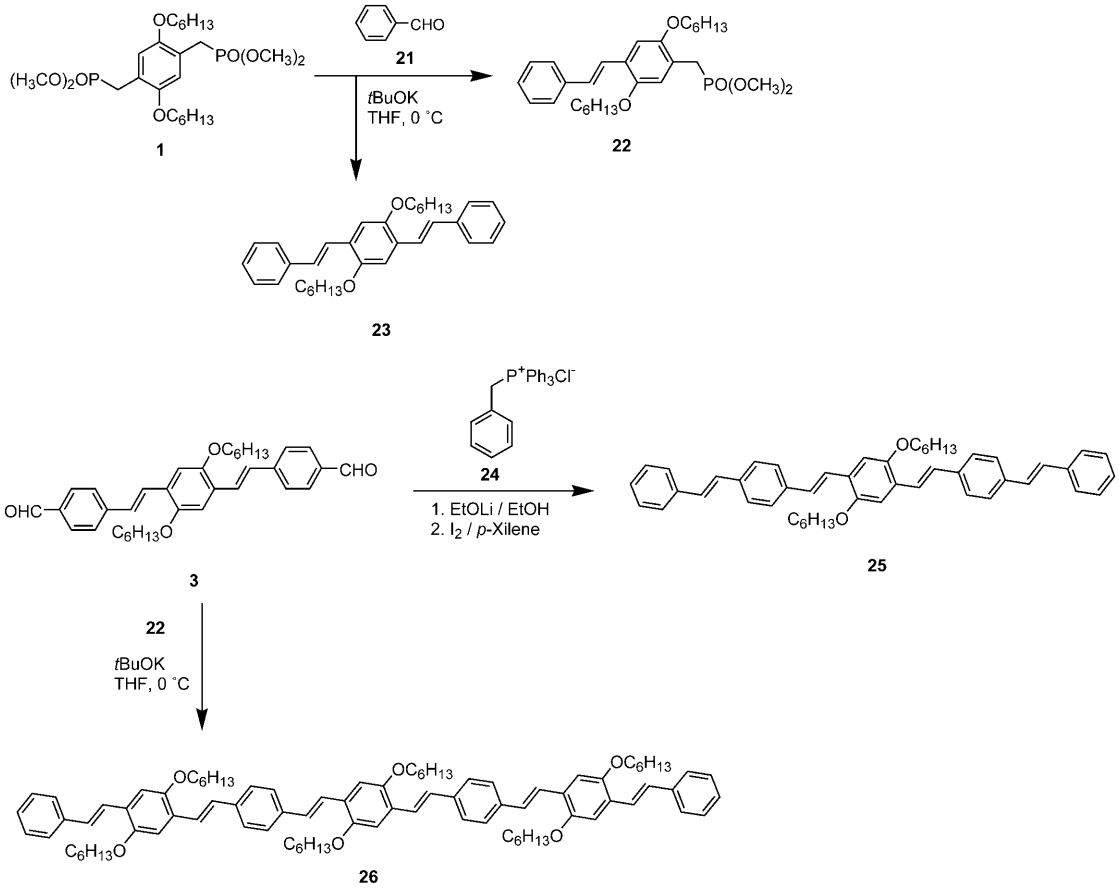

Scheme 5.

references. A better conjugation, stemming from orbital overlaps between the exTTF and the oligo-PPVs, is thought to be responsible for this effect. In parallel, the λ_{max} values of the diformyl-substituted oligo-PPVs increase from **3** (426 nm) to **6** (438 nm) and **8** (461 nm). exTTF–oligo-PPV systems (**10**, **11**–**13**, and **15** in Figure 1, bottom) show a similar trend.

Electrochemistry: All electrochemically determined redox potentials are collected in Table 1, including those of the unsubstituted trimer **23**, pentamer **25**, heptamer **26**, and *N*-methylpyrrolidino[3′,4′:1,2][60]fullerene (**27**) as reference systems.

Overall, the voltammograms of **16**–**20** indicate amphoteric redox behavior. Figure 2 shows, for example, one oxidation and four quasi-reversible reduction waves that correspond to the first oxidation of exTTF and to the first four reduction steps of C_{60}, respectively. The C_{60}-centered processes are similar to those found for the related unsubstituted C_{60} reference. However, the values are cathodically shifted relative to pristine C_{60} due to the saturation of a C_{60} double bond; this raises the LUMO energy of the resulting C_{60} derivative.[34] Previous electrochemical studies on oligo-PPVs documented their poor electron-accepting ability ($E^1_{red} \leq -2.0$ V vs Ag/AgCl) and confirmed that upon adding successive phenylenevinylene subunits the number of accessible redox states is enlarged.[35] In line with these considerations, the only observable oligo-PPV reduction was noted in **19** and **20**, with values that are similar to those observed for references **25** and **26** (Table 1).

On the oxidation side, a two-electron quasi-reversible oxidation forming the exTTF dication directly is observed at around 0.45 V. This feature was confirmed by Coulometric analysis[36] and other relevant studies.[37] Recent attempts to generate and characterize the exTTF radical cation caused the disproportionation of the dication species, which governs the instability of the radical cation.[38] In addition, a second oxidation wave appears at more positive values that corresponds to oligo-PPV-centered processes. With increasing conjugation length the oligo-PPV-centered processes shift cathodically, thus revealing the stronger electron-donor abilities of the larger oligomers.

Similar redox potentials, as found for the donor (exTTF) and acceptor (C_{60}), reveal, in agreement with the data stemming from the electronic spectra, only weak interactions between the redox chromophores in their ground state.

Theoretical calculations: The molecular structures of **19** and **20**, bearing pentameric and heptameric oligo-PPVs, respectively, were optimized by semi-empirical calculations at the

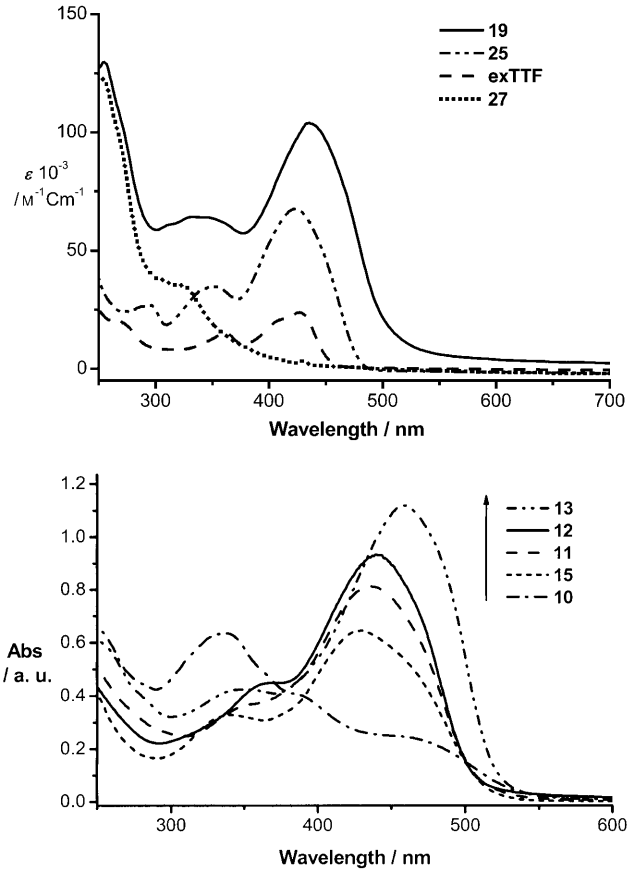

Figure 1. Top: UV-visible spectrum of triad **19** together with that of its building blocks (exTTF, pentamer **25**, and unsubstituted *N*-methylfulleropyrrolidine (**27**)) as a reference; bottom: UV-visible spectra of exTTF–oligoPPV dyads **10**–**13** and **15**.

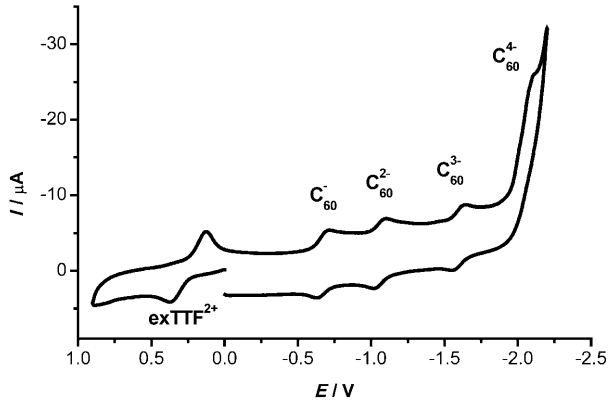

Figure 2. Voltammogram of **16** (see Table 1 for experimental conditions).

PM3 level. The alkoxy and oligoether chains were replaced by methyl groups to facilitate the theoretical calculations. Previous work has unequivocally shown that theoretical calculations carried out for exTTFs show a good agreement between theory and experiment, thereby demonstrating that the PM3 method provides a reasonably good description—even better than ab initio HF/6–31G* calculations—of the molecular structure of exTTFs.[39] Furthermore, the PM3 method has also proved its reliability for describing fullerene derivatives.[28,40]

As expected, our calculations show the butterfly-shaped nonplanar geometry of exTTF. The planar conformation of the exTTF moiety is strongly hindered by the short distance between the *peri*-hydrogen atoms and the sulfur atoms (1.78 Å). To avoid these interactions, the molecule adopts a distorted geometry forcing the central ring into a boat conformation (distance S···H = 2.48 Å).

The distortion from planarity is best described in terms of α and γ angles. While α corresponds to the angle formed by the benzene rings, γ defines the tilting of the dithiole units and is the supplement of the C7-C2-C5-C5 dihedral angle (Figure 3, left). In the most stable conformations, the calculated angles (**19**: $\alpha = 138.7°$ and $\gamma = 32.3°$; **20**: $\alpha = 138.4°$ and $\gamma = 32.8°$) are in good agreement with crystal packing in pristine exTTF[41] ($\alpha = 143.8°$ and $\gamma = 33.3°$) and those determined from theoretical calculations (PM3: $\alpha = 139.0°$ and $\gamma = 34.8°$; HF/6–31G*: $\alpha = 136.3°$ and $\gamma = 39.4°$; B3-P86/6–31G*: $\alpha = 142.1°$ and $\gamma = 34.0°$).

Figure 3 (right) shows the planarity of the oligo-PPV moiety, which spans a dihedral angle between the exTTF benzene ring and the benzene ring closest to the C_{60} unit of 9° for **19** and 38° for **20**. These findings are important, since they unambiguously confirm that the benzene ring of the exTTF unit is conjugated with the oligo-PPV moiety. Nevertheless, when comparing the heptamer-containing **20** with the pentamer-containing **19**, a strong deviation from planarity is found. To confirm these data, calculations were carried out on the nonsynthesized hexamer system **28** and, interestingly, an intermediate value of 25° was obtained.

Table 1. Redox potentials of **16**–**20**, oligo-PPVs **23**, **25**, and **26**, fulleropyrrolidine (**27**) and C_{60} (V vs SCE).[a]

Compound	Oxidation				Reduction				
	E^1_{pa}	E^2_{pa}	E^3_{pa}	E^4_{pa}	E^1_{pc}	E^2_{pc}	E^3_{pc}	E^4_{pc}	E^{olig}_{pc}
16	0.44	1.72	–	–	−0.70	−1.10	−1.64	−2.10	–
17	0.46	1.09	–	–	−0.68	−1.02	−1.66	−2.11	–
18	0.45	1.02	1.34	–	−0.70	−1.14	−1.70	−2.04	–
19	0.44	0.87	1.06	1.73	−0.70	−1.10	−1.65	−2.08	−1.88
20	0.47	0.80	1.59	–	−0.68	−1.07	−1.63	−2.06	−1.80
									−1.98
23	1.11	1.27	1.53	2.03	–	–	–	–	–
25	0.99	1.28	1.41	1.74	–	–	–	–	−1.94
26	0.88	1.35	1.65	–	–	–	–	–	−1.93
C_{60}	–	–	–	–	−0.60	−1.07	−1.64	−1.93	–
27	–	–	–	–	−0.69	−1.10	−1.65	−2.12	–

[a] GCE (glassy carbon) as working electrode, SCE as reference electrode, Bu_4NClO_4 (0.1 M) as supporting electrolyte, and *o*-dichlorobenzene/acetonitrile mixture (4/1 v/v) as solvent. Scan rate 200 mV s^{-1}.

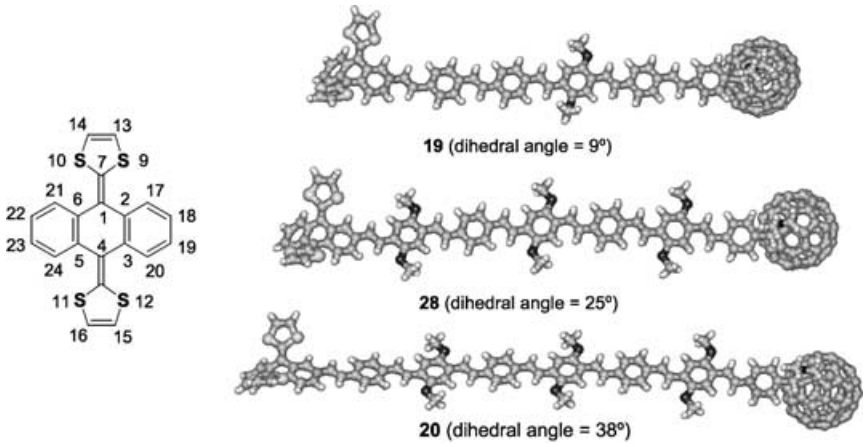

Figure 3. Left: Atom numbering used in the text. Right: Molecular modeling for triads **19**, **20**, and the nonsynthesized triad containing a hexamer oligo-PPV moiety (**28**).

Photophysics

References: In steady-state experiments, all reference compounds (i.e., oligo-PPVs **23**, **25**, and **26** and C_{60}) emit singlet excited state energy, although in different regions of the spectrum. While the fluorescence of oligo-PPV is typically observed in the 400–500 nm range, C_{60} emits with a maximum at 715 nm. The quantum yields range between 0.8 and 6×10^{-4} for the trimer and C_{60} reference, respectively.

Characteristic features were also noted in our ultrafast and fast transient absorption experiments (i.e., pico-, nano-, and microsecond time regime). We saw, for example, singlet excited states that are formed instantaneously: in the case of the oligo-PPV references (**23**, **25**, and **26**) singlet–singlet absorptions develop with maxima in the 500–600 nm range. For the C_{60} reference (**27**), on the other hand, the maximum is in the red at 880 nm. A fast intersystem crossing process ($k_{isc}\sim10^8\ s^{-1}$) governs the fate of the metastable singlet excited states in all references. The correspondingly formed triplet–triplet absorptions of the oligo-PPV and C_{60} references are all located in the range between 500 and 800 nm.

C_{60}–oligo-PPV: Relative to the strong and long-lived emission of the oligo-PPV references, the oligo-PPV emission in the C_{60}–oligo-PPV systems[40c] is quenched nearly quantitatively (see Table 2).

A familiar fullerene fluorescence spectrum was found with a 0→0 emission at 715 nm, despite exclusive excitation of the oligo-PPV moiety. To unravel the mechanism producing this emission, an excitation spectrum was recorded. The excitation spectra of the C_{60}–oligo-PPVs were found to be exact matches of the ground-state absorption of the oligo-PPV moieties. This implies a rapid transfer of singlet excited state energy from the photoexcited oligo-PPV to the covalently linked fullerene.[42]

As regards the picosecond transient absorption measurements, immediately after the 18 ps laser excitation of C_{60}–oligo-PPV broadly absorbing transients with maxima between 400 and 500 nm (i.e., singlet–singlet absorptions of the oligo-PPV) were found. The spectral features recorded right after the laser pulse clearly confirm, despite the presence of C_{60}, the successful formation of the oligo-PPV singlet excited state. While for the oligo-PPV references no significant decay of the excited state absorption was observed on the picosecond timescale (up to 6000 ps), C_{60}–oligo-PPV displays a drastically different kinetic behavior. In particular, the excited state absorption is short-lived with lifetimes (<25 ps) that corroborate the efficient emission quenching.

Once the rapid disappearance of the excited oligo-PPV absorption is complete (approx. 200 ps after the laser pulse), only characteristics of the fullerene singlet excited state absorption remain. The noted maximum at 880 nm is reminiscent of that found for the reference C_{60}. The singlet–singlet absorption reveals a two-step grow-in dynamics, in line with an energy-transfer mechanism. The faster process stems from the direct excitation of the C_{60} core, while the slower component is ascribed to the actual transfer of excited-state energy. The latter assignment is based on the nearly identical dynamics (<25 ps) observed for the second component relative to those of the decays at 500 nm.

Another process, whose outcome on the timescale of a few thousand picoseconds is the formation of a distinct, new maximum at 700 nm, follows the conclusion of the energy-transfer reaction in C_{60}–oligo-PPV. This absorption is in excellent agreement with the triplet excited state absorption of the C_{60} reference, which infers that the underlying reaction involves intersystem crossing from the C_{60} singlet to the energetically lower-lying triplet manifold.[43] A summary is given in Scheme 6.

C_{60}–oligo-PPV-ex*TTF*: The aforementioned energy transfer (see Scheme 6) is nearly quanti-

Table 2. Photophysical data of references and C_{60}–oligo-PPV.

	27	Trimer (**23**)	Pentamer (**24**)	C_{60} trimer	C_{60} pentamer
fluorescence maxima [nm]	–	445	485	472	503
fluorescence maxima [nm]	715	–	–	715	715
$\Phi_{FLUOR.}$ oligomer (toluene)	–	0.75	0.5	5.0×10^{-4}	5.8×10^{-4}
$\Phi_{FLUOR.}$ fullerene (toluene)	6.0×10^{-4}	–	–	6.0×10^{-4}	6.0×10^{-4}
ISC (toluene) [ns]	1.5	1.1	0.8	1.22	1.24
$k_{energy\ transfer}$ [s^{-1}]	–	–	–	$>4.0\times10^{10}$	$>4.0\times10^{10}$
τ_{FLUOR} fullerene (toluene) [ns]	1.5			1.48[a,b]	1.5[c,d]
triplet maxima [nm]	700	520	650	700	700

[a] Fluorescence lifetime in THF: 1.45 ns; [b] Fluorescence lifetime in benzonitrile: 1.05 ns; [c] Fluorescence lifetime in THF: 1.40 ns; [d] Fluorescence lifetime in benzonitrile: 0.95 ns.

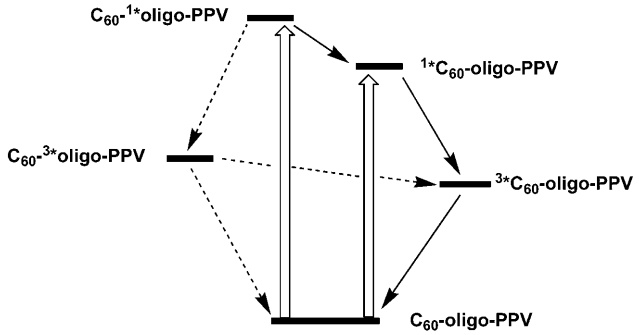

Scheme 6.

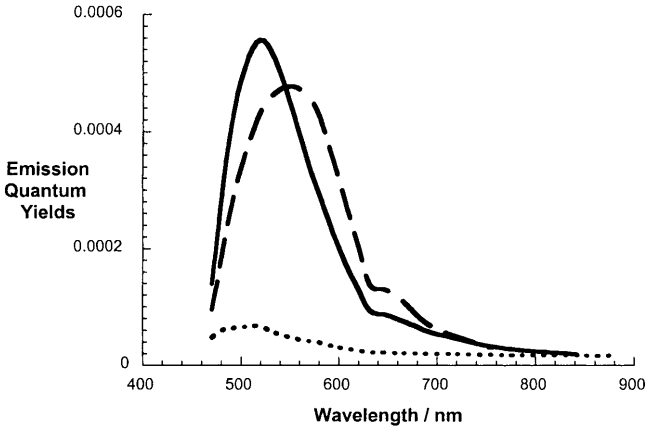

Figure 4. Fluorescence spectra (shown as quantum yields) of **16** (monomer, dotted line), **18** (trimer, full line), and **19** (pentamer, dashed line) in THF at room temperature, with matching absorption at the 450 nm excitation wavelength ($OD_{450}=0.2$).

tative in all C_{60}–oligo-PPVs and helps to concentrate the singlet excited state energy at the fullerene end. Notably, the contribution from an exothermic electron transfer is inappreciably small. This general pattern is not affected when linking exTTF to the other end of the wire to give C_{60}–oligo-PPV–exTTF, thus signifying that the singlet excited state energy trap is located at C_{60} (1.76 eV); we estimate the singlet excited state energy of exTTF to be around 2.6 eV. When exciting the oligo-PPV part in C_{60}–oligo-PPV–exTTF (in the 300–500 nm range), a rapid intramolecular transduction of energy, as evidenced by fluorescence quantum yields of about 5.0×10^{-4}, funnels the excited state energy to the C_{60} core and generates ^{1}*C_{60} with nearly 100% quantum yields.[44,45] Examples are illustrated in Figure 4 and summarized in Table 3.

Note that, in contrast to C_{60}–oligo-PPV, the C_{60}-centered fluorescence in Figure 4 is barely visible. The lack of quantitative C_{60} fluorescence suggests that exTTF enhances the fluorescence deactivation (vide infra). Excitation of C_{60} leads to a similar picture, namely notably reduced quantum yields.

To shed light on the nature of the product formed by this intramolecular deactivation, complementary time-resolved fluorescence and transient absorption measurements were necessary (i.e., with picosecond through millisecond time resolution) after 337 and/or 355 nm laser pulses.

Let's first direct our attention to the fluorescence lifetime measurements. In C_{60}–oligo-PPV–exTTF, a notable shortening of the C_{60} fluorescence lifetime is seen (see Table 3), which in THF reaches a factor of six relative to that seem for the C_{60} reference and C_{60}–oligo-PPV. Illustrations are given in Figure 5 for **16** and **19**.[46] Upon modifying the solvent polarity from THF ($\varepsilon=7.6$) and benzonitrile ($\varepsilon=24.8$) to DMF ($\varepsilon=36$) a gradual intensification of the quenching is discernible. We postulate that the underlying solvent dependence is due to an intramolecular electron transfer between the exTTF donor and the photoexcited C_{60} to yield $C_{60}^{\bullet-}$–oligo-PPV–exTTF$^{\bullet+}$.

On the other hand, in transient absorption measurements, detection of the two-step grow-in (at 18 ps) of the 880 nm absorption affirms the successful C_{60} singlet excited state formation in C_{60}–oligo-PPV–exTTF (not shown). However, instead of seeing the slow intersystem crossing dynamics, as for the C_{60} reference and the C_{60}–oligo-PPV, the singlet–singlet absorption decays faster in the presence of exTTF donors. The singlet excited state lifetimes, as determined

Table 3. Photophysical features of C_{60}–oligo-PPV–exTTF systems

	THF				Benzonitrile				DMF		
	Fluorescence lifetime[a] [ns]	Singlet lifetime[b] [ns]	Radical-pair lifetime[c] [ns]	Electronic coupling[d] [cm^{-1}]	Fluorescence lifetime[a] [ns]	Singlet lifetime[b] [ns]	Radical-pair lifetime[c] [ns]	Electronic coupling[d] [cm^{-1}]	Fluorescence lifetime[a] [ns]	Singlet lifetime[b] [ns]	Radical-pair lifetime[c] [ns]
16	0.26	0.32	295±15	5.3	0.16	0.18	430±20	6.2	≪0.1		
17	0.27	0.28	321±15	6.1	0.16	0.2	465±20	6.1	≪0.1	0.1	
18	0.27	0.33	365±15	6.9	0.17	0.2	499±25	5.9	0.09		650±30
19	0.3	0.35	411±20	5.8	0.18	0.21	557±25	5.5	0.11	0.13	
20	0.4	0.42	3190±150		0.28	0.25	4350±200		0.16	0.13	6100±300

[a] Determined by monitoring the fullerene fluorescence decay at 720 nm in time-resolved fluorescence lifetime measurements; [b] Determined by monitoring the fullerene singlet–singlet absorption at 900 nm in time-resolved transient absorption measurements; [c] Determined by monitoring both features of the radical ion pair state, that is, the 660 nm absorption maximum of the one-electron oxidized donor (exTTF) and the 1000 nm absorption maximum of the one-electron reduced acceptor (C_{60}) in time-resolved transient absorption measurements; [d] Determined from the following relation for a nonadiabatic electron transfer: $k_{et}=\left(\frac{4\pi3}{h^2\lambda k_B T}\right)^{1/2}V^2\exp\left[\frac{-\Delta G^{\ddagger}}{k_B T}\right]$, where h = Planck constant, k_B = Boltzmann constant (0.025 eV at 298 K), T = absolute temperature (298 K), λ = reorganization energy (1 eV), and $\Delta G^{\ddagger}$ = Gibbs activation energy, determined as: $\Delta G^{\ddagger}_{CS}=\frac{(\Delta G_{CS}+\lambda)^2}{4\lambda}$.

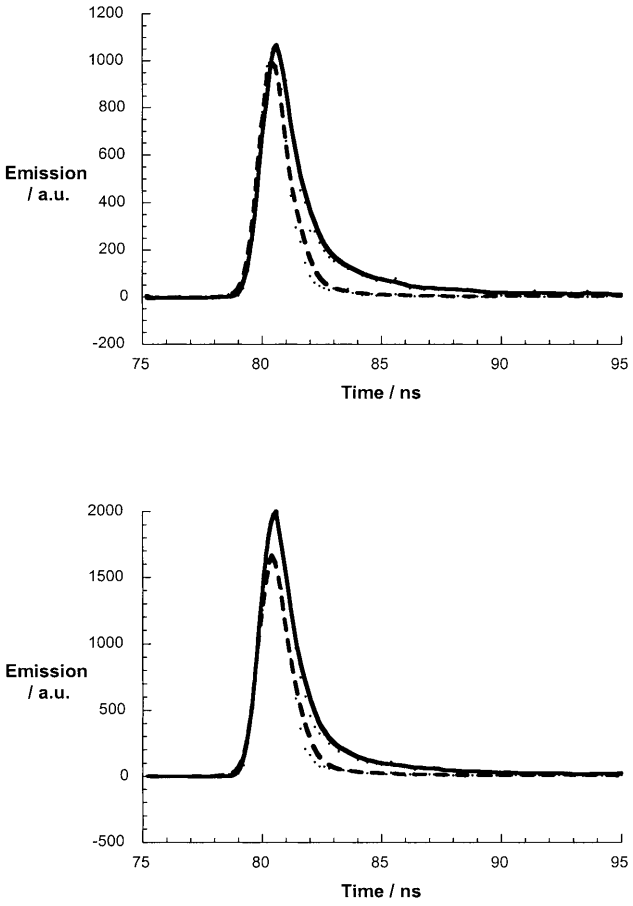

Figure 5. Fluorescence lifetime decays of **16** (monomer; top) and of **19** (pentamer; bottom) in THF (full lines), recorded at 720 nm, together with laser scatterer (dashed lines).

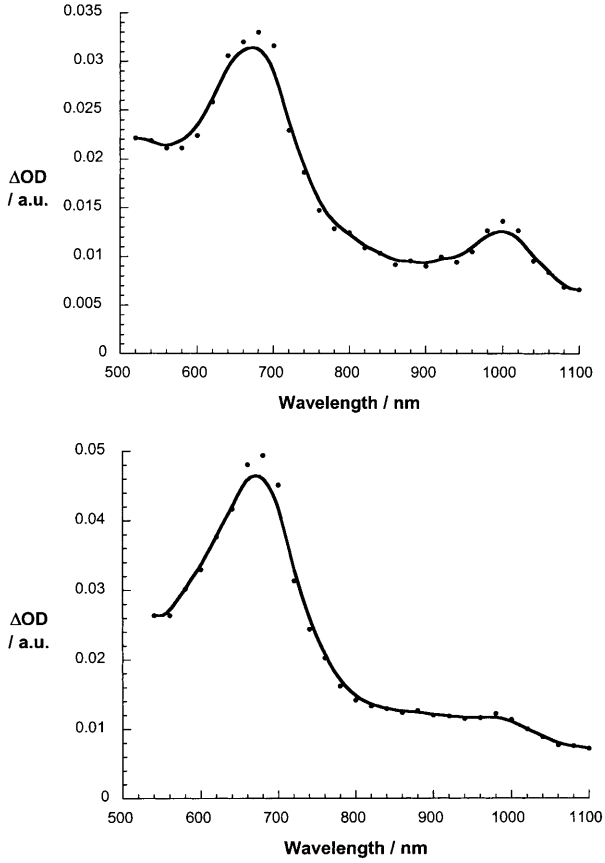

Figure 6. Differential absorption spectrum (visible and near-infrared) obtained upon nanosecond flash photolysis (355 nm) of approximately 1.0×10^{-5} M solutions of C_{60}–oligo-PPV–exTTF (**17**) in nitrogen-saturated THF with a time delay of 200 ns at room temperature (upper part) and of approximately 1.0×10^{-5} M solutions of C_{60}–oligo-PPV–exTTF (**20**) in nitrogen-saturated THF with a time delay of 200 ns at room temperature (lower part).

from an average of first-order fits of the time-absorption profiles at various wavelengths (850–950 nm), are listed in Table 3. An important aspect is that the singlet excited state lifetimes match quantitatively the values derived from the fluorescence experiments. Spectroscopically, the transient absorption changes, taken after the completion of the decay, bear no resemblance to the C_{60} triplet excited state (vide infra). Again, varying the solvent polarity from THF to DMF leads to an acceleration of the singlet deactivation. This supports our earlier hypothesis that an intramolecular electron transfer, yielding $C_{60}^{\bullet-}$–oligo-PPV–exTTF$^{\bullet+}$, governs the C_{60} singlet excited state deactivation.

Spectroscopic evidence for the radical-pair formation was found from the features developing in parallel with the disappearance of the C_{60} singlet–singlet absorption (see Figure 6). In the visible region, the observed maximum at 660 nm corresponds to the one-electron-oxidized π-radical cation of exTTF (exTTF$^{\bullet+}$), while in the near-infrared region the 1000 nm maximum resembles the signature of the one-electron-reduced form of C_{60} ($C_{60}^{\bullet-}$). Particularly striking is the fact that in the trimer-, pentamer-, and heptamer-based systems charge-separation occurs within a single step over remarkably long distances—no intermediate was observed that would suggest involvement of a transient oxidized $C_{60}^{\bullet-}$–oligo-PPV$^{\bullet+}$–exTTF oligomer.

The spectral fingerprints of the C_{60} π-radical anion (1000 nm; $\varepsilon\sim10\,000$ M^{-1}cm^{-1}) and that of the exTTF π-radical cation (665 nm; $\varepsilon\sim25\,000$ M^{-1}cm^{-1}) are useful probes to examine the charge-recombination dynamics. Both spectral attributes are persistent on the picosecond timescale and only start to decay slowly in the nanosecond regime. Time-absorption profiles, as depicted in Figure 7, illustrate that the $C_{60}^{\bullet-}$–oligo-PPV–exTTF$^{\bullet+}$ species decay in a single step. The charge recombination dynamics within these systems were determined accurately by fitting the decays of both fingerprints to a mono-exponential rate law.[47] To ensure a reliable interpretation of the data, the only fits admitted were those whose quality factor (reduced chi-square statistics, χ^2) was 0.98 or better.

The $C_{60}^{\bullet-}$–oligo-PPV–exTTF$^{\bullet+}$ radical pair in the monomer-based assembly is subject to a notable stabilization relative to the donor–acceptor system in which the anthracenoid part of the exTTF moiety is attached directly to the pyrrolidine functionality (C_{60}-exTTF). In benzonitrile, for instance,

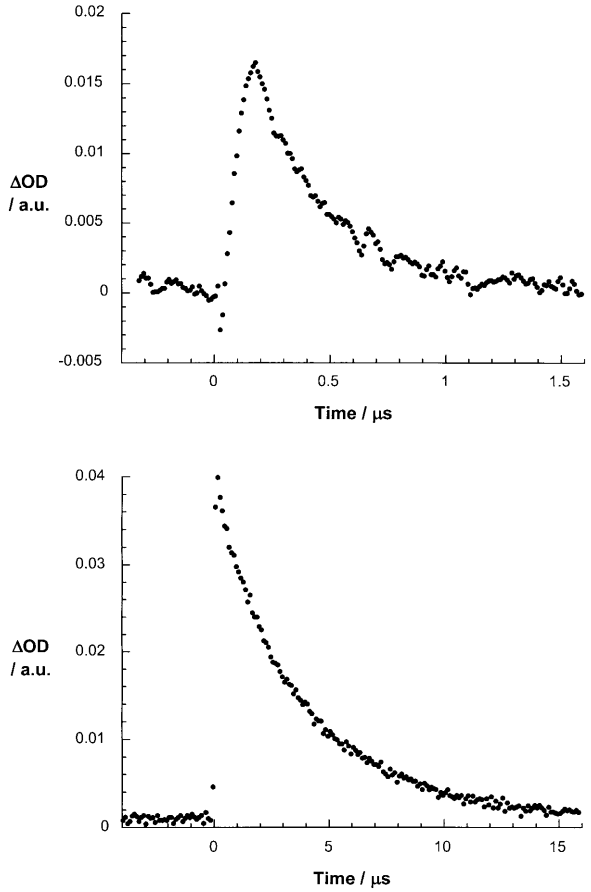

Figure 7. Time-absorption profiles at 1000 nm monitoring the $C_{60}^{\bullet-}$ decay dynamics in **16** (top) and **20** (bottom) obtained upon nanosecond flash photolysis (355 nm) of approximately 1.0×10^{-5} M deoxygenated benzonitrile solutions.

a lifetime of 204 ns has been found for this closely spaced system ($R_{CC}=9.7$ Å), whereas the monomer-based assembly (C_{60}–oligo-PPV–exTTF, **16**), with $R_{CC}=16.2$ Å, has a lifetime of 430 ns under the same experimental conditions. This reflects the larger separation and diminished electronic coupling. The use of a dimer-, trimer-, or pentamer-based oligo-PPV to integrate C_{60} and exTTF led to only marginal effects on the stability of the radical pair. To illustrate this phenomenon, lifetimes that range between 465 and 557 ns should be considered. However, radical-pair lifetimes about ten times longer were found for $C_{60}^{\bullet-}$–oligo-PPV–$exTTF^{\bullet+}$ (**20**), both in THF and benzonitrile.

Plotting the electron-transfer behavior as a function of donor–acceptor separation, except for the heptameric assembly, led to linear dependencies with THF and benzonitrile as solvents. From these plots, as shown in Figure 8, we determined the attenuation factors (β) for our assemblies as 0.01 ± 0.005 Å^{-1}, which are exceptionally small. Interestingly, fitting the charge separation the same way led to slightly lower β values (THF: 0.008 ± 0.005 Å^{-1}). We also used this method and the Marcus formalism for nonadiabatic electron transfer to assess the electronic coupling matrix element (V). Both approaches afforded nearly identical values

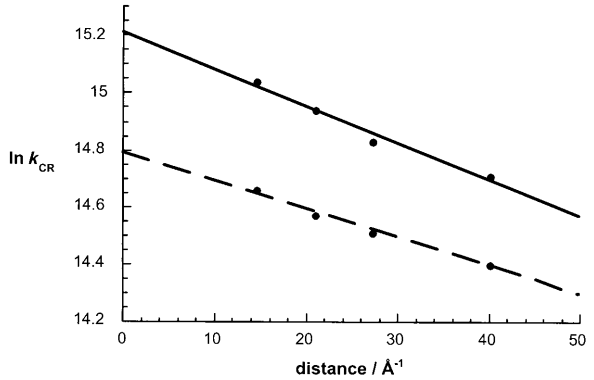

Figure 8. Dependence of electron-transfer rate constants (ln k_{CR}) for C_{60}–oligo-PPV–exTTF in nitrogen-saturated THF (solid line) and benzonitrile (dashed line) at room temperature on the center-to-center distances (R_{cc}). The lines represent the best fits ($\beta=0.01\pm0.005$ Å^{-1}, $V=2.3$ cm^{-1} in THF).

(2.3 cm^{-1} in THF; cf. the values listed in Table 3). Most importantly, the coupling in $C_{60}^{\bullet-}$–oligo-PPV–$exTTF^{\bullet+}$ (**19**), with values of 5.8 and 5.5 cm^{-1} in benzonitrile and THF, respectively, is unusually strong considering that a distance of 40 Å separates the electron donor from the electron acceptor. For comparison, the V-value for a molecular tetrad that spans over a similar distance is 1.6×10^{-4} cm^{-1}. The wirelike behavior in our C_{60}–oligo-PPV–exTTF can be best understood in terms of the π-conjugation effective between the anthracenoid part of the donor, the oligo-PPV bridge, and the pyrrolidine ring of the C_{60} derivative.[48]

To analyze the charge-recombination mechanism we probed the radical-pair lifetimes between 272 and 350 K, which are summarized in Figure 9. The Arrhenius plots for the monomer, dimer (not shown), and trimer can be separated into two distinct sections: the low-temperature regime (<320 K) and the high-temperature regime (>320 K). The weak temperature-dependence in the 272 to 320 K range suggests that a stepwise charge-recombination via a transi-

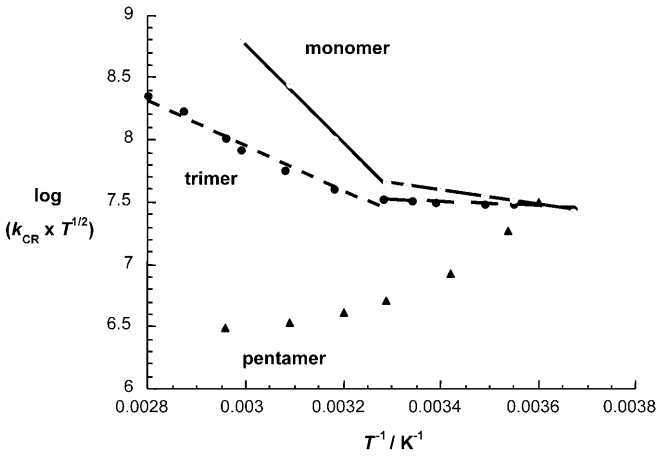

Figure 9. Arrhenius analyses of the temperature-dependent electron-transfer rate constants (k_{CR}) for **16**, **18**, and **19** in deoxygenated benzonitrile.

ent $C_{60}^{\bullet-}$–oligo-PPV$^{\bullet+}$–exTTF species can be ruled out, leaving electron tunneling via superexchange as the operative mode. This picture is in sound agreement with the thermodynamic barrier that must be overcome to form $C_{60}^{\bullet-}$–oligo-PPV$^{\bullet+}$–exTTF. At higher temperatures (>320 K) this picture changes and the charge recombination is accelerated. The strong temperature-dependence observed suggests a thermally activated charge recombination. The activation barriers (E_a), derived from the slopes (**16**: 0.8 eV; **18**: 0.6 eV; **19**: 0.5 eV), confirm the HOMO(C_{60})–HOMO(wire) energy gap. Interestingly, $C_{60}^{\bullet-}$–oligo-PPV–exTTF$^{\bullet+}$ (**19**) reveals the opposite trend: the charge recombination slows down substantially in the high-temperature region. A temperature-induced decoupling, for example, by effecting an orbital alignment in the oligo-PPV bridge, is thought to be responsible for the slow-down of the charge recombination.

Finally, comparing solvents of different polarity, namely THF, benzonitrile, and DMF, stabilizing effects for all $C_{60}^{\bullet-}$–exTTF$^{\bullet+}$ radical pairs were seen for the more-polar solvents.[20–22] Since better solvation of the radicals, which is particularly important in polar media, lowers the energy of the charge-separated state, this trend suggests charge-recombination dynamics that are in the normal region of the Marcus parabola. We believe that two aspects are responsible for the overall observation. Firstly, due to the low oxidation potential of the donor the driving forces are kept quite low, relative, for example, to those assumed for metalloporphyrin-based analogues. Secondly, the structural changes of the donor, which accompany the oxidation, attenuate the reorganization energy of the donor–acceptor system.

A superexchange mechanism leading directly to $C_{60}^{\bullet-}$–oligo-PPV–exTTF$^{\bullet+}$ (see Figure 10) is imposed in **16** by the large HOMO(C_{60})–HOMO(wire) gap of 0.7 eV. In **17**–**20**, however, good electronic mixing of these two HOMOs, which have nearly isoenergetic levels, diminishes the energy penalty for initial electron injection from the wire to ^{1}*C_{60}. Paraconjugation, which extends into the exTTF donor, and the exothermic nature of the charge-shift reaction are then responsible for extremely fast charge-shift dynamics to form $C_{60}^{\bullet-}$–oligo-PPV–exTTF$^{\bullet+}$.

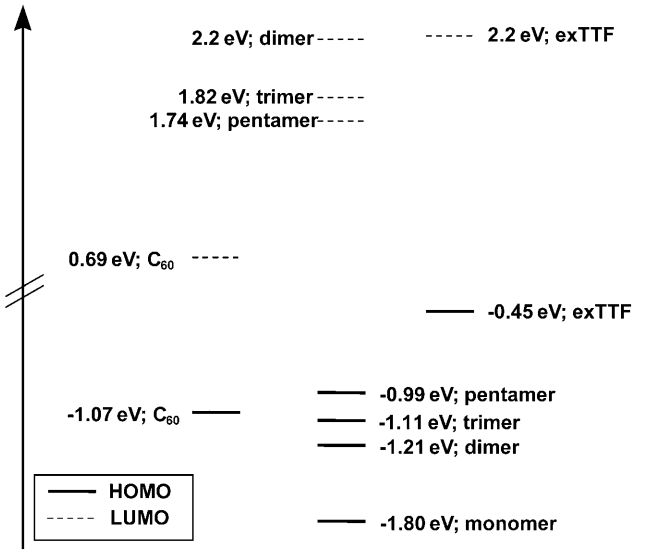

Figure 10. HOMO (solid line) and LUMO (traced line) levels of C_{60}, oligomers, and exTTF (determination was carried out as reported in reference [5]).

In principle, two different transfer processes may contribute to the charge recombination. Figure 10 shows that large LUMO(C_{60})–LUMO(wire) gaps of at least 1.1 eV result exclusively in an electron tunneling mechanism. Charge transfer from the HOMO at C_{60} (i.e., $C_{60}^{\bullet-}$) to the HOMO at exTTF (i.e., exTTF$^{\bullet+}$), on the other hand, may proceed by superexchange or hopping. In fact, the temperature dependence helps to recognize the interplay between both processes. Once the hopping mechanism dominates, especially in **18** and **19**, and the hole migrates first to the wire, good HOMO(C_{60})–HOMO(wire) energy matching and strong electronic coupling lead to a kinetically fast and spectroscopically unresolvable recovery of the ground state.

Conclusion

In summary, we have carried out the rational design of linear donor–acceptor arrays by integrating fully conjugated oligomers with a well-defined length and constitution. The novel compounds were prepared by a convergent synthetic strategy involving iterative olefination Wittig–Horner reactions and a final Prato reaction to introduce the C_{60} unit into the final molecular arrays (**16**–**20**).

The electrochemical study reveals an amphoteric redox behavior and a lack of significant electronic communication between the donor (exTTF) and the acceptor (C_{60}) moieties through the π-conjugated oligomer in the ground state; this was also confirmed by the electronic spectra. However, we have succeeded in demonstrating photoinduced electron transfer over distances of up to 50 Å with formation of the respective radical pairs ($C_{60}^{\bullet-}$–oligo-PPV–exTTF$^{\bullet+}$). The charge-recombination dynamics show the presence of highly stabilized charge-separated states with lifetimes in the range between 465 ns and 557 ns in benzonitrile, which indicates a very low influence of the oligomer length on the electron rate. These findings, as well as the very low value determined for the attenuation factor ($\beta = 0.01 \pm 0.005$ Å^{-1}), clearly indicate a nanowire behavior. A longer radical-pair lifetime (10 times) was observed for the heptamer-containing array $C_{60}^{\bullet-}$–oligo-PPV–exTTF$^{\bullet+}$, which has been accounted for by the loss of planarity of the oligomer moiety, with calculated (PM3) dihedral angles between the two terminal benzenes of 38°. The strong electron coupling between the donor and acceptor moieties through the π-conjugated oligomer, with coupling constants of about 5.5 cm^{-1}, is particularly important for the observed wire-like behavior. These results open the way to use the current examples as integrated components in the construction of optoelectronic devices and nanotechnology.

Experimental Section

Picosecond laser flash photolysis experiments were carried out with 355 nm laser pulses from a mode-locked, Q-switched Quantel YG-501 DP Nd:YAG laser system (pulse width 18 ps, 2–3 mJ per pulse). Nanosecond laser studies were performed with laser pulses from a Molectron UV-400 nitrogen laser system (337.1 nm, 8 ns pulse width, 1 mJ per pulse) or from a Qunta-Ray CDR Nd: YAG system (355 nm, 20 ns pulse width). The photomultiplier output was digitized with a Tektronix 7912 AD programmable digitizer. The quantum yields of the triplet excited states ($\Phi_{TRIPLET}$) were determined by the triplet–triplet energy transfer method using β-carotene as an energy acceptor. For all photophysical experiments an error of 10% must be considered.

Fluorescence lifetimes were measured with a laser strobe fluorescence lifetime spectrometer (Photon Technology International) with 337 nm laser pulses from a nitrogen laser fiber-coupled to a lens-based T-formal sample compartment equipped with a stroboscopic detector. Details of the laser strobe systems are described on the manufacturer's web site (http://www.pti-nj.com).

Emission spectra were recorded with an SLM 8100 Spectrofluorometer. The experiments were performed at room temperature. When measuring the fullerene emission in the 700 nm region, a 570 nm long-pass filter in the emission path was used in order to eliminate the interference from the solvent and stray light for recording the fullerene fluorescence. Each spectrum is an average of at least five individual scans and the appropriate corrections were applied. The fluorescence quantum yields were determined with respect to a 9,10-diphenylanthracene reference (Aldrich, 99+%) ($\Phi=1$) and are an average value of three fluorophore concentrations with ODs at an excitation wavelength ranging from 0.1 to 0.5.

All solvents were dried and distilled according to standard procedures. Reagents were used as purchased. All air-sensitive reactions were carried out under an argon atmosphere. Flash chromatography was performed on silica gel 60 Å (Merck, 40–60 μm). TLC was performed on silica gel 60 F_{254} coated aluminum sheets (Merck) with detection by UV at 254 nm. Melting points were determined on a Gallenkamp apparatus. NMR spectra were recorded on Bruker AC-200 (^{1}H: 200 MHz; ^{13}C: 50 MHz), Bruker AC-300 or Varian XL-300 (^{1}H: 300 MHz; ^{13}C: 75 MHz), or Bruker DRX-500 or AMX-500 (^{1}H: 500 MHz; ^{13}C: 125 MHz) spectrometers at 298 K using partially deuterated solvents as internal standards. Coupling constants (J) are denoted in hertz and chemical shifts (δ) in ppm. FT-IR spectra were recorded on a Nicolet-Magna-IR 5550 spectrometer. Electrospray ionization (ESI) mass spectra were recorded on a HP1100 MSD spectrometer.

General procedure for Wittig–Horner olefination: Potassium *tert*-butoxide was added portionwise to a solution of the corresponding phosphonate and aldehyde in dry THF under argon. The mixture was stirred at 0°C for 90 min and then methanol (10 mL) was added. The mixture was extracted twice with dichloromethane, the combined organic layers were dried over magnesium sulfate, and the solvent was removed under vacuum to yield a residue which was purified by chromatography as described in each case.

Where deprotection of an aldehyde functionality was required, the crude was dissolved in chloroform, a 1 N solution of HCl was added, and the mixture stirred overnight.

Compound 7: Potassium *tert*-butoxide was added portionwise (180 mg, 1.6 mmol) to a stirred solution of compound **1** (2.0 g, 3.8 mmol) in dry THF (120 mL). After 20 min a solution of compound **2** (265 mg, 1.3 mmol) in dry THF (50 mL) was added dropwise. After 2 h, workup was carried out according to the general procedure. The residue was purified by chromatography on silica gel (hexane/dichloromethane 2:3; dichloromethane; dichloromethane/methanol 100:1) to yield compound **7** (313 mg, 41%) as a yellow oil. ^{1}H NMR ($CDCl_3$, 200 MHz, 25°C): $\delta=$ 7.86 (d, $^3J_{H,H}=8.1$ Hz, 2H), 7.64 (d, $^3J_{H,H}=8.1$ Hz, 2H), 7.60 (d, $^3J_{H,H}=$ 16.1 Hz, 1H), 7.14 (d, $^3J_{H,H}=16.1$ Hz, 1H), 7.08 (s, 1H), 6.94 (s, 1H), 5.30 (s, 1H; -CH(OEt)$_2$), 4.01 (t, $^3J_{H,H}=6.3$ Hz, 4H), 3.74 (q, $^3J_{H,H}=6.8$ Hz, 4H), 3.69 (d, $^3J_{H,P}=11.0$ Hz, 6H), 3.27 (d, $^3J_{H,P}=22.0$ Hz, 2H), 1.82 (m, 4H), 1.54–1.28 (m, 12H), 1.24 (t, $^3J_{H,H}=6.8$ Hz, 6H), 0.91 ppm (m, 6H); ^{13}C NMR ($CDCl_3$, 75 MHz, 25°C): $\delta=150.92$, 150.77, 144.28, 144.15, 135.09, 134.32, 130.21, 129.49, 128.41, 127.27, 125.12, 115.93, 110.91, 65.40, 69.13, 68.18, 31.58, 29.68, 29.43, 25.88, 22.61, 14.00 ppm; FTIR (KBr): $\tilde{\nu}=$ 2848, 1604, 1512, 1450, 1225, 1036, 870, 812 cm^{-1}; UV/Vis (CH_2Cl_2): λ_{max} (ε) = 297 (19000), 350 nm (18200 mol^{-1}cm^{3}dm^{-1}); MS (EI): m/z (%): 604 (100) [M^+], 559 (35), 445 (15), 362 (13), 251 (18).

Compound 8: 2,5-Bis[(1*E*)-2′-(4-formylphenyl)vinyl]-1,4-dihexyloxybenzene (**3**; 100 mg, 0.19 mmol) was treated with **7** (230 mg, 0.38 mmol), according to the general procedure, to afford 191 mg (76%) of **8** as an orange solid (silica gel; hexane/dichloromethane, 7:3). ^{1}H NMR ($CDCl_3$, 200 MHz, 25°C): $\delta=10.00$ (s, 2H; -CHO), 7.88 (d, $^3J_{H,H}=8.3$ Hz, 4H), 7.67 (d, $^3J_{H,H}=8.3$ Hz, 4H), 7.61 (s, 2H), 7.54 (s, 8H), 7.52 (d, $^3J_{H,H}=$ 16.3 Hz, 4H), 7.18 (d, $^3J_{H,H}=16.3$ Hz, 4H), 7.17 (d, $^3J_{H,H}=16.3$ Hz, 2H), 7.15 (d, $^3J_{H,H}=16.3$ Hz, 2H), 7.14 (s, 4H), 4.08 (m, 12H), 1.90 (q, $J=$ 6.6 Hz 12H), 1.57–1.26 (m, 36H), 0.95 ppm (m, 18H); ^{13}C NMR ($CDCl_3$, 75 MHz, 25°C): $\delta=191.59$, 151.53, 151.19, 151.08, 144.21, 137.38, 137.01, 135.09, 130.23, 129.03, 128.07, 127.28, 12.14, 127.00, 126.90, 126.82, 125.89, 123.37, 123.04, 110.90, 110.58, 110.43, 69.63, 69.52, 31.64, 29.47, 25.98, 22.66, 14.05 ppm; FTIR (KBr): $\tilde{\nu}=2930$, 2906, 2858, 1697 (CHO), 1624, 1595, 1491, 1423, 1384, 1207,1035, 961 cm^{-1}; UV/Vis (CH_2Cl_2): λ_{max} (ε) = 246 (67600), 340 (69200), 461 nm (269000 mol^{-1}cm^{3}dm^{-1}); MS(ESI): m/z (%): 1370 (100) [M^++Na].

General procedure for the preparation of exTTF-OPPV dyads 10–13 and 15: Triphenylphosphonium salt **9** (0.22 mmol) and potassium *tert*-butoxide (54 mg, 0.48 mmol) were dissolved in toluene and heated to reflux. After 1 h a solution of the corresponding aldehyde (**2**, **3**, **6**, or **8**; 0.33–0.44 mmol) in toluene was added with a syringe in one portion and the reaction was kept under reflux for 12 h. After the reaction reached room temperature, methanol was added (5 mL), the solvent was removed under vacuum, and the resulting mixture was treated with 2.0 N HCl, washed with water, and extracted with dichloromethane. The organic layer was dried with magnesium sulfate and the solvent was removed under vacuum. The resulting solid was purified by silica gel chromatography using hexane/dichloromethane as eluent to afford a dark-red solid.

Compound 10: 61% yield; m.p.: 192–194°C; ^{1}H NMR ($CDCl_3$, 200 MHz, 25°C): $\delta=9.93$ (s, 1H), 7.87 (d, $^3J_{H,H}=7$ Hz, 3H), 7.70 (t, $^3J_{H,H}=7$ Hz, 4H), 7.47 (m, 1H), 7.33 (t, $^3J_{H,H}=7$ Hz, 1H), 7.19 (t, $^3J_{H,H}=7$ Hz, 4H), 6.33 ppm (s, 4H); ^{13}C NMR ($CDCl_3$, 50 MHz, 25°C): $\delta=191.5$, 144.7, 135.9, 135.6, 135.3, 132.9, 131.9, 130.2, 130.1, 1129.9, 129.8, 127.2, 126.9, 126.0, 125.4, 124.9, 123.2, 117.3, 116.9 ppm; FTIR (KBr): $\tilde{\nu}=3421$, 2924, 2852, 1695, 1541, 1508, 1195, 1165, 964 cm^{-1}; UV/Vis (CH_2Cl_2): λ_{max} (ε) = 246 (676000), 337 (645600), 387 (417000), 454 nm (251200 mol^{-1}cm^{3}dm^{-1}); MS(EI): m/z (%): 510 (100) [M^+], 306 (4), 94 (18), 69 (32).

Compound 11: 32% yield (37% based on recovered starting material); m.p: 182–184°C; ^{1}H NMR ($CDCl_3$, 200 MHz, 25°C): $\delta=9.92$ (s, 1H; -CHO), 7.80 (t, $^3J_{H,H}=4$ Hz, 4H), 7.60 (m, 5H), 7.55 (d, $^3J_{H,H}=7$ Hz, 2H), 7.47 (s, 4H), 7.38 (t, $^3J_{H,H}=7$ Hz, 2H), 7.23 (m, 2H), 7.07 (m, 4H), 6.24 (s, 4H), 4.06 (m, 4H), 1.88 (m, 4H; -CH$_2$-), 1.59 (s, 2H;) 1.40 (m, 4H), 1.25 (s, 4H), 0.88 ppm (m, 6H; -CH$_3$); ^{13}C NMR ($CDCl_3$, 50 MHz, 25°C): $\delta=191.6$, 151.5, 151.1, 144.2, 137.2, 136.7, 136.3, 135.8, 135.3, 135.1, 134.8, 130.2, 128.3, 128.0, 126.9, 126.8, 126.0, 125.9, 125.0, 117.3, 117.2, 114.0, 110.5, 110.4, 69.5, 53.4, 31.6, 29.7, 26.0, 22.6, 14.0 ppm; FTIR (KBr): $\tilde{\nu}=3448$, 2924, 2852, 1691, 1595, 1508, 1211, 1029, 956 cm^{-1}; UV/Vis (CH_2Cl_2): λ_{max} (ε) = 242 (9100), 354 (6300), 434 nm (13800 mol^{-1}cm^{3}dm^{-1}); MS (ESI): m/z (%): 914 (100) [M^+], 856 (17), 744 (80), 685 (80), 643 (40). elemental analysis calcd (%) for $C_{57}H_{54}O_3S_4$: C 74.83, H 5.95; found: C 75.21, H 6.29.

Compound 12: 27% yield (61% based on recovered starting material); m.p.: 276–277°C (decomp); ^{1}H NMR ($CDCl_3$, 200 MHz, 25°C): $\delta=10.00$ (s, 1H; -CHO), 7.87 (t, $^3J_{H,H}=8$ Hz, 2H), 7.84 (s, 1H), 7.67 (t, $^3J_{H,H}=$ 7 Hz, 5H), 7.53 (m, 8H), 7.49 (m, 4H), 7.41 (d, $^3J_{H,H}=8$ Hz, 2H), 7.31 (d, $^3J_{H,H}=8$ Hz, 2H), 7.25 (m, 3H), 7.13 (m, 8H), 6.33 (s, 4H), 4.07 (m, 4H), 1.90 (m, 4H; -CH$_2$-), 1.59–1.25 (m, 12H), 0.89 ppm (m, 6H; -CH$_3$); ^{13}C NMR ($CDCl_3$, 50 MHz, 25°C): $\delta=190.2$, 150.1, 142.5, 137.4, 136.4, 134.9, 134.6, 134.5, 130.9, 129.3, 128.9, 127.4, 127.2, 126.4, 125.9, 125.8, 125.0, 124.7, 124.0, 123.1, 122.4, 121.2, 116.3, 109.4, 68.5, 31.1, 30.8, 28.9, 28.7, 28.6, 25.2, 21.9, 13.3 ppm; FTIR (KBr): $\tilde{\nu}=2923$, 2852, 2164, 1685,

1570, 1205, 758 cm^{-1}; UV/Vis (CH_2Cl_2): λ_{max} (ε) = 244 (44700), 367 (42600), 440 nm (89100 $mol^{-1}cm^3dm^{-1}$); MS (ESI): *m/z* (%): 1118 (100) [M^+], 1033 (18); elemental analysis calcd (%) for $C_{73}H_{66}O_3S_4$: C 78.31, H 5.94; found: C 77.89, H 6.37.

Compound 13: 25% yield (34% based on recovered starting material); ^{1}H NMR ($CDCl_3$, 300 MHz, 25°C): δ = 10.00 (s, 1H), 7.89–7.85 (m, 3H), 7.73–7.61 (m, 3H), 7.54–7.45 (m, 21H), 7.34–7.29 (m, 2H), 7.22–7.11 (m, 14H), 6.33 (s, 4H), 4.08 (t, $^3J_{H,H}$ = 6.3 Hz, 12H), 1.90 (q, J = 6.6 Hz, 12H), 1.57–1.25 (m, 36H), 0.95 ppm (m, 18H); ^{13}C NMR ($CDCl_3$, 75 MHz, 25°C): δ = 191.66, 151.49, 151.14, 151.04, 144.20, 137.37, 137.17, 136.96, 136.52, 135.81, 135.78, 135.67, 135.35, 135.29, 135.25, 135.20, 135.16, 135.04, 134.72, 130.91, 130.25, 129.01, 128.83, 128.39, 128.35, 128.14, 128.02, 127.24, 127.11, 127.00, 126.96, 126.83, 125.99, 125.82, 125.30, 125.01, 124.95, 124.28, 123.34, 123.18, 122.97, 122.81, 117.31, 117.25, 117.11, 110.81, 110.49, 110.33, 69.57, 69.46, 31.92, 31.65, 29.70, 29.48, 29.36, 25.98, 22.67, 14.13, 14.07 ppm; FTIR (KBr): $\tilde{\nu}$ = 2954, 2923, 2853, 1782, 1596, 1464, 1377, 1262, 1207, 1073, 961, 721 cm^{-1}; UV/Vis (CH_2Cl_2): λ_{max} (ε) = 48 (29500), 351 (23400), 459 nm (64500 $mol^{-1}cm^3dm^{-1}$); MS (ESI): *m/z* (%): 1723 (100) [M^++H].

Compound 15: Potassium *tert*-butoxide (240 mg, 2.10 mmol) was added portionwise to a solution of **14** (133 mg, 0.25 mmol) and phosphonate **7** (88 mg, 0.25 mmol) in dry THF (35 mL) under argon. The mixture was stirred at room temperature for 16 h and then methanol (10 mL) was added. The solvent was removed under reduced pressure, the resulting mixture was dissolved in dichloromethane (50 mL), and 1 M HCl (50 mL) was added. The mixture was stirred at room temperature for 16 h and then, after separation, the organic layers were dried over magnesium sulfate and the solvent was removed under vacuum to yield a solid residue, which was purified by chromatography (silica gel, hexane/dichloromethane 1/1) to yield 115 mg (66%) of **15** as a red solid. ^{1}H NMR ($CDCl_3$, 300 MHz, 25°C): δ = 10.00 (s, 1H), 7.87 (d, $^3J_{H,H}$ = 8 Hz, 3H), 7.73–7.61 (m, 6H), 7.55 (d, $^3J_{H,H}$ = 16.6 Hz, 1H), 7.50 (d, $^3J_{H,H}$ = 16.6 Hz, 1H), 7.30 (m, 2H), 7.27 (d, $^3J_{H,H}$ = 16.1 Hz, 2H), 7.15 (d, $^3J_{H,H}$ = 4.6 Hz, 2H), 6.32 (s, 4H), 4.08 (q, J = 6.1 Hz, 4H), 1.90 (q, J = 6.3 Hz, 4H), 1.56–1.26 (m, 12H), 0.95 ppm (m, 6H); ^{13}C NMR ($CDCl_3$, 75 MHz): δ = 191.59, 151.55, 151.12, 144.23, 135.80, 135.64, 135.59, 135.31, 135.28, 135.08, 134.69, 130.23, 129.05, 128.09, 127.24, 127.18, 126.82, 125.97, 125.89, 125.28, 124.97, 124.35, 123.40, 122.92, 122.26, 117.30, 117.24, 117.04, 110.92, 110.48, 69.63, 69.55, 31.71, 31.62, 29.54, 29.44, 26.02, 25.97, 22.69, 22.65, 14.11, 14.03 ppm; FTIR (KBr): $\tilde{\nu}$ = 2954, 2924, 2853, 1630, 1593, 1493, 1421, 1208, 1163, 964, 801, 649 cm^{-1}; UV/Vis (CH_2Cl_2) λ_{max} = 229, 339, 429 nm; MS (ESI): *m/z* (%): 812 (100) [M^+], 704 (15).

General procedure for the preparation of exTTF–oPPV–C_{60} triads 16–20: The corresponding aldehyde (**6**, **8**, **10**, **12**, and **16**; 0.05 mmol), [60]fullerene (38 mg, 0.05 mmol), and the respective amino acid [sarcosine, *N*-(3,6,9-trioxadecyl)glycine, or *N*-octylglycine; 0.15–0.25 mmol] were dissolved in toluene or chlorobenzene (30 mL) and the mixture was refluxed for 24 h. After this time, the reaction was allowed to reach room temperature, and then the solvent was partially vacuum evaporated and then poured onto a silica-gel column. The black solid obtained after chromatography was further purified by repeated centrifugation in methanol and diethyl ether to yield the corresponding triads as black solids.

Compound 16: Eluent: toluene/ethyl acetate (9:1); 17% yield; m.p.: > 300°C; ^{1}H NMR ($CDCl_3$, 500 MHz, 25°C): δ = 7.83 (s, 2H), 7.70 (m, 3H), 7.59 (d, $^3J_{H,H}$ = 5 Hz, 2H), 7.38 (d, $^3J_{H,H}$ = 5 Hz, 1H), 7.28 (m, 2H), 7.17 (s, 1H), 7.16 (d, $^3J_{H,H}$ = 16.3 Hz, 1H), 7.14 (d, $^3J_{H,H}$ = 16.3 Hz, 1H), 6.29 (s, 4H), 5.35 (s, 1H; CH_2-N-), 5.30 (s, 1H), 3.99 (s, 1H), 3.82 (d, $^3J_{H,H}$ = 4 Hz, 2H), 3.79 (d, $^3J_{H,H}$ = 4 Hz, 2H), 3.72 (t, $^3J_{H,H}$ = 5 Hz, 4H), 3.57 (t, $^3J_{H,H}$ = 5 Hz, 4H), 3.36 ppm (s, 3H); ^{13}C NMR ($CDCl_3$, 125 MHz, 25°C): δ = 147.29, 146.26, 146.13, 145.89, 145.53, 145.29, 144.70, 144.56, 144.31, 143.09, 142.95, 142.55, 142.14, 142.04, 141.60, 141.46, 140.09, 139.87, 139.55, 137.84, 135.80, 135.65, 135.52, 135.22, 134.88, 134.77, 130.00, 129.71, 129.19, 128.99, 128.19, 128.00, 126.95, 125.98, 125.27, 124.91, 124.38, 122.86, 121.99, 117.23, 117.08, 82.30, 71.99, 70.68, 70.64, 70.60, 68.82, 65.75, 59.08, 52.39, 48.67 ppm; FTIR (KBr): $\tilde{\nu}$ = 3434, 2921, 2851, 1632, 1508, 1455, 1107, 527 cm^{-1}; UV/Vis (CH_2Cl_2): λ_{max} (log ε) = 57 (6.85), 326 (6.58), 378 (6.29), 432 (shoulder, 6.14), 441 nm (6.13); MS (ESI): *m/z* (%): 1389 (100) [M^+], 1219 (65), 551 (62).

Compound 17: Eluent: hexane/toluene (1:1); 47% yield; ^{1}H NMR ($CDCl_3/CS_2$, 500 MHz, 25°C): δ = 8.33–8.22 (m, 4H), 7.87–7.63 (m, 6H), 7.53 (d, J = 8.3 Hz, 2H), 7.43 (d, $^3J_{H,H}$ = 16.4 Hz, 1H), 7.22 (d, $^3J_{H,H}$ = 16.4 Hz, 1H), 7.08 (d, $^3J_{H,H}$ = 16.6 Hz, 2H), 7.04 (s, 1H), 6.76 (s, 4H), 5.10 (d, $^3J_{H,H}$ = 9.2 Hz, 1H), 5.05 (s, 1H), 4.12 (d, $^3J_{H,H}$ = 9.2 Hz, 1H), 4.04 (m, 4H), 3.25 (m, 1H), 2.56 (m, 1H), 1.88 (m, 6H), 1.55–1.24 (m, 22H), 0.92 ppm (m, 9H); ^{13}C NMR ($CDCl_3/CS_2$, 125 MHz, 25°C): δ = 156.26, 153.97, 153.30, 151.30, 150.74, 147.08, 146.60, 146.26, 146.03, 145.72, 145.57, 145.30, 145.03, 144.48, 144.18, 143.78, 142.96, 142.80, 142.38, 142.09, 141.93, 141.81, 141.49, 141.35, 140.00, 139.74, 139.37, 137.74, 136.67, 136.51, 136.39, 135.64, 135.53, 133.80, 133.67, 133.57, 133.39, 131.61, 130.83, 129.56, 128.69, 127.74, 126.99, 126.62, 125.43, 124.86, 123.48, 118.21, 110.53, 109.95, 82.28, 69.06, 68.69, 66.72, 32.04, 31.70, 29.81, 29.49, 28.50, 27.66, 26.02, 22.91, 22.84, 14.28, 14.16 ppm; FTIR (KBr): $\tilde{\nu}$ = 2921, 2853, 1632, 1505, 1460, 1107, 527 cm^{-1}. UV/Vis (CH_2Cl_2) λ_{max} (ε) = 56 (309000), 328 (131800), 397 (shoulder, 69200), 431 (53700), 451 nm (49000 $mol^{-1}cm^3dm^{-1}$); MS (ESI): *m/z* (%): 1659 (100) [M^+ +H], 1573 (52), 1432 (17).

Compound 18: Eluent: cyclohexane/toluene (3:7); 19% yield; m.p.: > 300°C; ^{1}H NMR ($CDCl_3/CS_2$, 500 MHz, 25°C): δ = 8.29 (m, 2H), 7.89 (m, 2H), 7.80 (t, $^3J_{H,H}$ = 5 Hz, 3H), 7.62 (m, 1H), 7.53 (m, 3H), 7.47 (m, 2H), 7.44 (t, $^3J_{H,H}$ = 5 Hz, 2H), 7.41 (s, 1H), 7.35 (s, 1H), 7.23 (m, 2H), 7.05 (d, $^3J_{H,H}$ = 16.7 Hz, 2H), 7.03 (s, 1H), 7.01 (d, $^3J_{H,H}$ = 16.7 Hz, 1H), 6.31 (s, 4H), 5.01 (d, $^3J_{H,H}$ = 9.5 Hz, 1H; CH_2-N-), 4.97 (s, 1H; -CH-N-), 4.30 (d, $^3J_{H,H}$ = 9.5 Hz, 1H; CH_2-N-),4.04 (t, $^3J_{H,H}$ = 6 Hz, 4H), 2.87 (s, 3H; N-CH_3), 1.89 (m, 4H), 1.58 (m, 4H), 1.57–1.27 (m, 8H), 0.97 ppm (m, 6H); ^{13}C NMR ($CDCl_3/CS_2$, 125 MHz, 25°C): δ = 156.04, 153.85, 153.34, 153.10, 151.06, 147.31, 146.73, 146.36, 146.25, 146.18, 145.97, 145.66, 145.59, 145.41, 145.28, 144.74, 144.70, 144.42, 143.20, 143.05, 142.73, 142.63, 142.28, 142.20, 142.09, 141.97, 141.73, 141.61, 140.27, 140.03, 139.68, 138.63, 138.37, 136.98, 136.70, 135.87, 135.79, 135.43, 133.93, 133.80, 133.73, 132.74, 132.07, 131.57, 131.35, 129.63, 129.37, 128.05, 127.60, 127.26, 127.08, 127.02, 126.76, 126.63, 126.54, 126.39, 126.02, 124.85, 124.26, 124.18, 124.13, 118.43, 118.27, 110.23, 83.10, 76.85, 69.66, 68.89, 68.58, 39.75, 32.10, 29.93, 26.42, 23.28, 14.57 ppm; FTIR (KBr): $\tilde{\nu}$ = 2923, 2852, 1633, 1556, 1421, 1033, 876, 796, 526, 468 cm^{-1}; UV/Vis (CH_2Cl_2): λ_{max} (ε) = 56 (107100), 327 (46800), 413 nm (38900 $mol^{-1}cm^3dm^{-1}$); MS (ESI): *m/z* (%): 1661 (95) [M^+], 1619 (100), 1577 (62), 1332 (37), 806 (31).

Compound 19: Eluent: toluene/ethyl acetate (9:1); 27% yield; m.p.: 216–219°C; ^{1}H NMR ($CDCl_3/CS_2$, 500 MHz, 25°C): δ = 8.42 (m, 1H), 8.26 (m, 2H), 7.91 (m, 2H), 7.80 (m, 1H), 7.66 (t, $^3J_{H,H}$ = 7 Hz, 2H), 7.55 (d, $^3J_{H,H}$ = 7 Hz, 4H), 7.49 (m, 9H), 7.38 (m, 3H), 7.27 (m, 4H), 7.10 (m, 7H), 6.32 (s, 4H), 5.35 (s, 1H; CH_2-N-), 5.30 (s, 1H; CH-N-), 4.41 (s, 1H; CH-N-), 4.04 (t, $^3J_{H,H}$ = 6 Hz, 4H), 3.83 (d, $^3J_{H,H}$ = 5 Hz, 2H), 3.79 (d, $^3J_{H,H}$ = 5 Hz, 2H), 3.73 (t, $^3J_{H,H}$ = 5 Hz, 4H), 3.57 (t, $^3J_{H,H}$ = 5 Hz, 4H), 3.37 (s, 3H; N-CH_3), 1.89 (m, 4H), 1.57 (m, 4H), 1.41–1.26 (m, 8H), 0.89 ppm (m, 6H); ^{13}C NMR ($CDCl_3/CS_2$, 125 MHz, 25°C): δ = 150.16, 146.37, 145.56, 145.37, 145.21, 144.99, 144.88, 144.63, 144.37, 144.31, 143.79, 143.67, 143.41, 142.21, 142.05, 141.67, 141.25, 141.14, 141.00, 140.70, 140.57, 139.18, 138.98, 138.65, 137.12, 137.02, 136.65, 136.47, 136.13, 135.52, 135.28, 135.12, 134.75, 134.62, 133.42, 132.94, 130.87, 130.71, 130.47, 129.83, 129.64, 129.83, 129.10, 128.76, 128.50, 128.24, 128.06, 127.84, 127.30, 127.08, 127.03, 126.86, 126.58, 126.39, 126.29, 125.97, 125.56, 125.05, 124.01, 123.47, 123.17, 122.60, 117.24, 116.76, 116.36, 109.43, 82.28, 71.98, 70.62, 69.34, 58.94, 52.45, 30.87, 28.93, 28.70, 25.19, 21.94, 13.27 ppm; FTIR (KBr): $\tilde{\nu}$ = 3434, 2921, 2852, 1631, 1461, 1419, 1178, 1106, 957, 525 cm^{-1}; UV/Vis (CH_2Cl_2): λ_{max} (ε) = 55 (19500), 311 (shoulder, 91200), 333 (95500), 435 nm (155000 $mol^{-1}cm^3dm^{-1}$); MS (ESI): *m/z* (%): 1998 (36) [M^+], 1913 (100), 1827 (85), 1738 (35), 1597 (27).

Compound 20: Eluent: hexane/toluene (1:1); 30% yield; m.p.: > 300°C; H NMR ($CDCl_3/CS_2$, 500 MHz, 25°C): δ = 7.79 (m, 3H), 7.65 (m, 3H), 7.56–7.42 (m, 17H), 7.41 (d, $^3J_{H,H}$ = 16.3 Hz, 4H), 7.30 (m, 2H), 7.13 (s, 2H), 7.10 (s, 4H), 7.09 (d, $^3J_{H,H}$ = 15.3 Hz, 4H), 7.08 (d, $^3J_{H,H}$ = 16.3 Hz, 4H), 6.32 (s, 4H), 5.13 (d, $^3J_{H,H}$ = 9.2 Hz, 1H), 5.07 (s, 1H), 4.14 (d, $^3J_{H,H}$ = 9.2 Hz, 1H), 4.05 (q, J = 6.3 Hz, 12H), 3.28 (m, 1H), 2.59 (m, 1H), 1.90 (m, 14H), 1.60–1.26 (m, 46H), 0.98 ppm (m, 21H); ^{13}C NMR

($CDCl_3/CS_2$, 125 MHz, 25 °C): δ = 156.31, 154.01, 153.36, 153.28, 150.87, 147.09, 146.63, 146.29, 145.96, 145.74, 145.59, 145.05, 144.50, 144.21, 142.97, 142.82, 142.39, 142.11, 141.94, 141.83, 141.49, 141.36, 140.00, 139.77, 139.40, 137.95, 136.98, 136.65, 136.42, 136.34, 136.25, 135.92, 135.63, 135.08, 134.53, 129.55, 128.10, 126.70, 126.45, 126.33, 125.88, 125.17, 124.79, 124.15, 123.70, 123.03, 122.74, 121.95, 117.16, 117.07, 110.15, 110.00, 82.32, 69.16, 68.7, 66.73, 53.39, 53.13, 32.04, 31.74, 30.13, 29.81, 29.57, 28.50, 27.66, 26.75, 26.06, 22.85, 14.28, 14.16 ppm; FTIR (KBr): $\tilde{\nu}$ = 2923, 2853, 1632, 1461, 1422, 1178, 1107, 957, 527 cm^{-1}; UV/Vis (CH_2Cl_2): λ_{max} (ε) = 54 (141200), 330 (30200), 458 nm (155000 $mol^{-1} cm^3 dm^{-1}$).

Compound 25: Dialdehyde **3** (60 mg, 0.11 mmol) and lithium ethoxide (1 M, 0.22 mL, 0.22 mmol) were added to a stirred solution of triphenylphosphonium salt **24** (65 mg, 0.22 mmol) in dry ethanol (20 mL) at 50 °C under argon. After 3 h the solvent was vacuum evaporated, and the residue was suspended in xylene (10 mL) and heated to reflux for 24 h after addition of a catalytic amount of iodine. After the reaction mixture had cooled, methanol was added to form a precipitate, which was purified by chromatography (silica gel, hexane/dichloromethane 4:1) to yield 42 mg (54 %) of **25** (all-*E* isomer) as a yellow solid. ^{1}H NMR ($CDCl_3$, 200 MHz, 25 °C): δ = 7.53 (s, 8H), 7.52 (d, $^3J_{H,H}$ = 16.5 Hz, 4H), 7.39 (m, 4H), 7.30 (d, $^3J_{H,H}$ = 16.5 Hz, 2H), 7.29 (d, $^3J_{H,H}$ = 1.3 Hz, 2H), 7.23 (t, $^3J_{H,H}$ = 1.3 Hz, 1H), 7.14 (d, $^3J_{H,H}$ = 16.5 Hz, 2H), 7.13 (s, 6H), 4.07 (t, $^3J_{H,H}$ = 6.4 Hz, 4H), 1,90 (q, $^3J_{H,H}$ = 6.4 Hz, 4H), 1.60–1.25 (m, 8H), 0.93 ppm (t, J = 6.8 Hz, 6H); ^{13}C NMR ($CDCl_3$, 50 MHz, 25 °C): δ = 151.16, 137.41, 137.38, 136.47, 128.69, 128.41, 128.36, 127.60, 126.95, 126.83, 126.49, 123.41, 110.57, 69.59, 31.65, 29.48, 25.98, 22.66, 14.07 ppm; FTIR (KBr): $\tilde{\nu}$ = 2925, 2854, 1591, 1512, 1491, 1423, 1387, 1261, 1202, 1047, 980, 810, 750, 688 cm^{-1}; MS (EI): m/z (%): 686 (100) [M^+], 510 (7) [$M^+ - 2(C_6H_{13})$], 286 (28), 207 (51), 149 (29); UV/Vis (CH_2Cl_2): λ_{max} (ε) = 36 (30900), 296 (13200), 354 (20400), 424 nm (40700 $mol^{-1} cm^3 dm^{-1}$).

Compound 26: Following the general procedure for Wittig–Horner olefination, compound **3** (100 mg, 0.19 mmol) was treated with compound **22** (230 mg, 0.38 mmol) to afford 65 mg (50 %) of **26** as an orange solid (silica gel, hexane/dichloromethane 7/3). ^{1}H NMR ($CDCl_3$, 200 MHz, 25 °C): δ = 7.53 (s, 12H), 7.52 (d, $^3J_{H,H}$ = 16.4 Hz, 6H), 7.48–7.28 (m, 6H), 7.15 (s, 6H), 7.14 (d, $^3J_{H,H}$ = 16.4 Hz, 6H), 4.07 (t, $^3J_{H,H}$ = 6.3 Hz, 12H), 1,89 (q, $^3J_{H,H}$ = 6.3 Hz, 12H), 1.55–1.26 (m, 36H), 0.95 ppm (t, J = 6.8 Hz, 18H); ^{13}C NMR ($CDCl_3$, 50 MHz, 25 °C): δ = 151.21, 138.02, 137.21, 128.79, 128.64, 128.46, 127.04, 126.99, 126.84, 126.53, 123.57, 123.29, 110.76, 110.67, 69.67, 31.66, 29.59, 25.98, 22.67, 14.04 ppm; FTIR (KBr): ν = 2928, 2857, 1586, 1492, 1464, 1422, 1341, 1258, 1207, 961, 691 cm^{-1}; UV/Vis (CH_2Cl_2): λ_{max} (ε) = 44 (31600), 328 (38900), 450 nm (151300 $mol^{-1} cm^3 dm^{-1}$); MS (ESI): m/z (%): 1291 (100) [M^++H].

Acknowledgements

Financial support for this project came from the MCYT of Spain (Project BQU2002-00855). Part of this work was also supported by the Office of Basic Energy Sciences of the U.S. Department of Energy (Contribution No. NDRL-4602 from the Notre Dame Radiation Laboratory).

[1] a) F. L. Carter, *Molecular Electronic Devices*, Dekker, New York, **1987**; b) *Photoinduced Electron Transfer* (Eds.: M. A. Fox, M. Channon), Elsevier, Amsterdam, **1988**; c) *Electron Transfer in Chemistry* (Ed.: V. Balzani), Wiley-VCH, Weinheim, **2001**.

[2] a) P. F. Barbara, T. J. Meyer, M. A. Ratner, *J. Phys. Chem.* **1996**, *100*, 13148–13168; b) H. M. McConnell, *J. Chem. Phys.* **1961**, *35*, 508–515.

[3] a) M. D. Newton, *Chem. Rev.* **1991**, *91*, 767; b) D. Gust, T. A. Moore, A. L. Moore, *Acc. Chem. Res.* **1993**, *26*, 198–205; c) M. N. Paddon-Row, *Acc. Chem. Res.* **1994**, *27*, 18–25; d) I. R. Gould, S. Farid, *Acc. Chem. Res.* **1996**, *29*, 522–528; e) V. Balzani, A. Juris, M. Venturi, S. Campagna, S. Serroni, *Chem. Rev.* **1996**, *96*, 759–834; f) I. Willner, *Acc. Chem. Res.* ***1997***, *30*, 347–356; g) P. Piotrowiak, *Chem. Soc. Rev.* **1999**, *28*, 143–150; h) H. Kurreck, M. Huber, *Angew. Chem.* **1995**, *107*, 929–947; *Angew. Chem. Int. Ed. Engl.* **1995**, *34*, 849–866.

[4] a) M. R. Wasielewski, *Chem. Rev.* **1992**, *92*, 435–461; b) G. B. Schuster, *Acc. Chem. Res.* **2000**, *33*, 253–260; c) P. J. Bracher, D. Schuster, in *Fullerenes: From Synthesis to Optoelectronic Properties* (Eds.: D. M. Guldi, N. Martín), Kluwer Academic, Dordrecht, The Netherlands, **2002**, pp. 163–212.

[5] H. B. Gray, J. R. Winkler, *Annu. Rev. Biochem.* **1996**, *65*, 537–561.

[6] T. S. Arrhenius, M. Blanchard-Desce, M. Dvolaitzky, J.-M. Lehn, J. Malthête, *Proc. Natl. Acad. Sci. USA* **1986**, *83*, 5355–5359.

[7] a) R. E. Halmlin, P. J. Danliker, J. K. Barton, *Angew. Chem.* **1997**, *109*, 2830–2848; *Angew. Chem. Int. Ed. Engl.* **1997**, *36*, 2714–2730; b) T. J. Meade, J. F. Kayyem, *Angew. Chem.* **1995**, *107*, 358–360; *Angew. Chem. Int. Ed. Engl.* **1995**, *34*, 352–354.

[8] a) *Molecular Electronics* (Eds.: J. Jortner, M. Ratner), Blackwell, Oxford, **1997**; b) *An Introduction to Molecular Electronics* (Eds.: M. C. Petty, M. R. Bryce, D. Bloor), Oxford University Press, New York, **1995**.

[9] a) J. R. Heath, M. A. Ratner, *Phys. Today* **2003**, *56*, 43–49; b) C. Joachim, J. K. Gimzewski, A. Aviram, *Nature* **2000**, *408*, 541–548; c) P. F. H. Schwab, M. D. Levin, J. Michl, *Chem. Rev.* **1999**, *99*, 1863–1934; d) E. A. Weiss, M. J. Ahrens, L. E. Sinks, A. V. Gusev, M. A. Ratner, M. R. Wasielewski, *J. Am. Chem. Soc.* **2004**, *126*, 5577–5584; e) R. L. McCreery, *Chem. Mater.* **2004**, *16*, 4477–4496.

[10] a) J. M. Tour, *Chem. Rev.* **1996**, *96*, 537–553; b) M. D. Ward, *Chem. Soc. Rev.* **1995**, *24*, 121–134; c) J. M. Tour, *Acc. Chem. Res.* **2000**, *33*, 791–804.

[11] a) P. F. H. Schwab, M. D. Levin, J. Michl, *Chem. Rev.* **1999**, *99*, 1863–1933; b) R. E. Martin, T. Mäder, F. Diederich, *Angew. Chem.* **1999**, *111*, 834–838; *Angew. Chem. Int. Ed.* **1999**, *38*, 817–821.

[12] For a review on functionalized oligomers, see: J. L. Segura, N. Martín, *J. Mater. Chem.* **2000**, *10*, 2403–2435.

[13] J.-M. Lehn, *Supramolecular Chemistry, Concepts and Perspectives*, VCH, Weinheim, **1995**, Chapter 8.

[14] For a recent review on molecular electronics, see: R. L. Carroll, C. B. Gorman, *Angew. Chem.* **2002**, *114*, 4556–4579; *Angew. Chem. Int. Ed.* **2002**, *41*, 4378–4400; .

[15] a) *Electronic Materials: The Oligomer Approach* (Eds.: K. Müllen, G. Wegner) Wiley-VCH, Weinheim, **1998**; b) R. E. Martin, F. Diederich, *Angew. Chem.* **1999**, *111*, 1440–1469; *Angew. Chem. Int. Ed.* **1999**, *38*, 1350–1377; ; c) J.-F. Nierengarten, *Sol. Energy Mater. Sol. Cells* **2004**, *83*, 187–199; d) J. L. Segura, N. Martín, D. M. Guldi, *Chem. Soc. Rev.* **2005**, *34*, 31–47.

[16] A. Hradsky, B. Bildstein, N. Schuler, H. Schottenberger, P. Jaitner, K.-H. Ongania, K. Wurst, J.-P. Launay, *Organometallics* **1997**, *16*, 392–402.

[17] N. Ono, H. Tomita, K. Maruyama, *J. Chem. Soc. Perkin Trans. 1* **1992**, 2453–2456.

[18] W. B. Davis, W. A. Svec, M. A. Ratner, M. R. Wasielewski, *Nature* **1998**, *396*, 60–63.

[19] G. Pourtis, D. Beljonne, J. Cornil, M. A. Ratner, J. L. Brédas, *J. Am. Chem. Soc.* **2002**, *124*, 4436–4447.

[20] a) M. A. Herranz, N. Martín, *Org. Lett.* **1999**, *1*, 2005–2007; b) N. Martín, L. Sánchez, D. M. Guldi, *Chem. Commun.* **2000**, 113–114; c) M. A. Herranz, N. Martín, J. Ramey, D. M. Guldi, *Chem. Commun.* **2002**, 2968–2969; d) N. Martín, L. Sánchez, D. M. Guldi, *J. Phys. Chem. A* **2000**, 104, 4648–4657; e) S. González, N. Martín, A. Swartz, D. M. Guldi, *Org. Lett.* **2003**, *5*, 557–560.

[21] L. Sánchez, I. Pérez, N. Martín, D. M. Guldi, *Chem. Eur. J.* **2003**, *9*, 2457–2468.

[22] a) J. L. Segura, N. Martín, *Tetrahedron Lett.* **1999**, *40*, 3239–3242; b) J. L. Segura, R. Gómez, N. Martín, C. Luo, D. M. Guldi, *Chem. Commun.* **2000**, 701–702; c) D. M. Guldi, C. Luo, A. Swartz, R. Gómez, J. L. Segura, N. Martín, C. Brabec, N. S. Sariciftci, *J. Org. Chem.* **2002**, *67*, 1141–1152; d) C. Atienza, B. Insuasty, C. Seoane, N. Martín, J. Ramey, D. M. Guldi, *J. Mater. Chem.* **2005**, *15*, 124–132.

[23] a) J. L. Segura, R. Gómez, N. Martín, D. M. Guldi, A. Swartz, C. Luo, *Chem. Commun.* **2001**, 707–708; b) D. M. Guldi, A. Swartz, C. Luo, R. Gómez, J. L. Segura, N. Martín, *J. Am. Chem. Soc.* **2002**, *124*, 10875–10886.
[24] A preliminary communication has been published recently: F. Giacalone, J. L. Segura, N. Martín, D. M. Guldi, *J. Am. Chem. Soc.* **2004**, *126*, 5340–5341.
[25] G. Drehfahl, R. Kühmstedt, H. Oswald, H.-H. Hörhold, *Makromol. Chem.* **1970**, *131*, 89.
[26] Compound **4** was obtained in a one-step Arbuzov reaction by refluxing commercially available 4-(bromomethyl)benzonitrile in trimethylphosphite. For a review of the Arbuzov reaction, see: A. K. Bhattacharya, G. Thyagarajan, *Chem. Rev.* **1981**, *81*, 415–430.
[27] A similar approach towards soluble oligo(*p*-phenylenevinylene) derivatives that bear functional groups at both termini through the use of Wittig–Horner olefinations has been developed in parallel to our work, see: C. Xue, F.-T. Luo, *J. Org. Chem.* **2003**, *68*, 4417–4421.
[28] S. González, N . Martín, D. M. Guldi, *J. Org. Chem.* **2003**, *68*, 779–791.
[29] A. W. Johnson, in *Ylides and Imines of Phosphorous*, Wiley, New York, **1993**, Chapters 3 and 9.
[30] Small amounts of the respective oligomers bearing two exTTF units resulting from a twofold Wittig reaction were characterized by mass spectrometry.
[31] N. Martín, I. Pérez, L. Sánchez, C. Seoane, *J. Org. Chem.* **1997**, *62*, 5690–5695.
[32] a) M. Prato, M. Maggini, *Acc. Chem. Res.* **1998**, *31*, 519–526; b) N. Tagmatarchis, M. Prato, *Synlett* **2003**, 768–779.
[33] Compound **23** has been synthesized previously by a different synthetic strategy involving a twofold Heck reaction: Z. H. Peng, A. R. Gharavi, L. P. Yu, *J. Am. Chem. Soc.* **1997**, *119*, 4622–4632.
[34] L. Echegoyen, L. E. Echegoyen, *Acc. Chem. Res.* **1998**, *31*, 593–601.
[35] a) J. Heinze, J. Mortensen, K. Müllen, R. Schenk, *J. Chem. Soc. Chem. Commun.* **1987**, 701–703; b) R. Schenk, H. Gregorius, K. Meerholz, J. Heinze, K. Müllen, *J. Am. Chem. Soc.* **1991**, *113*, 2634–2647.
[36] M. R. Bryce, A. J. Moore, *J. Chem. Soc. Perkin Trans. 1* **1991**, 157–168.
[37] a) N. Martín, E. Ortí, in *Handbook of Advanced Electronic and Photonic Materials and Devices* (Ed.: H. S. Nalwa), Academic Press, New York, **2001**, Vol. 3, Chapter 6; b) I. Pérez, S.-C. Liu, N. Martín, L. Echegoyen, *J. Org. Chem.* **2000**, *65*, 3796–3803.
[38] a) D. M. Guldi, L. Sánchez, N. Martín, *J. Phys. Chem. B* **2001**, *105*, 7139–7144; b) A. E. Jones, C. A. Christensen, D. F. Perepichka, A. S. Batsanov, A. Beeby, P. J. Low, M. R. Bryce, A. W. Parker, *Chem. Eur. J.* **2001**, *7*, 973–978.
[39] N. Martín, L. Sánchez, C. Seoane, E. Ortí, P. M. Viruela, R. Viruela, *J. Org. Chem.* **1998**, *63*, 1268–1279.
[40] a) F. Giacalone, J. L. Segura, N. Martín, *J. Org. Chem.* **2002**, *67*, 3529–3532; b) M. C. Díaz, M. A. Herranz, B. M. Illescas, N. Martín, N. Godbert, M. R. Bryce, C. Luo, A. Swartz, G. Anderson, D. M. Guldi, *J. Org. Chem.* **2003**, *68*, 7711–7721; c) G. de la Torre, F. Giacalone, J. L. Segura, N. Martín, D. M. Guldi, *Chem. Eur. J.* **2005**, *11*, 1267–1280.
[41] M. R. Bryce, A. J. Moore, M. Hasan, G. J. Ashwell, A. T. Fraser, W. Clegg, M. B. Hursthouse, A. I. Karanlov, *Angew. Chem.* **1990**, *102*, 1493–1495; *Angew. Chem. Int. Ed. Engl.* **1990**, *29*, 1450–1452.
[42] The fullerene fluorescence lifetimes in C_{60}-wire are virtually identical to what is seen in the C_{60} reference.
[43] The transient absorption changes, recorded about 50 ns after 6 ns laser excitation, also reveal the attributes for the C_{60} triplet excited state.
[44] Involvement of the oligomer units in initiating electron-transfer processes is unlikely due to their unfavorably high oxidation potentials (see electrochemistry section). For further details see our previous papers in references [22,23].
[45] Although exTTF references emit around 475 nm, which correlates to a singlet excited state energy of about 2.6 eV, the donor emission remains nearly unaffected in C_{60}–wire–exTTF. This suggests that exTTFs, once photoexcited, fail to contribute notably to the overall electron and energy transfer reactivity.
[46] The C_{60} reference reveals nearly solvent-independent fluorescence lifetimes (τ) of 1.5 ns.
[47] the fact that the decay of both probes is similar and gives rise to kinetics that obey a clean unimolecular rate law is important.
[48] Also in line with the good electronic couplings are the comparable charge-separation quantum yields (THF: $62\pm4\%$; benzonitrile: $42\pm3\%$; DMF: $35\pm3\%$), which again support the mediating effect of the oligo(phenylenevinylene) systems, despite the large distances (R_{CC} values of 40 Å).

Received: January 21, 2005
Published online: June 1, 2005